

# Testing BSM Higgs self-couplings via $HHH$ $\nu\nu$ production at future $e^-e^+$ colliders

Paula Martínez Suárez

Máster en Física Teórica



MÁSTERES  
DE LA UAM  
2019 – 2020

Facultad de Ciencias



# Testing BSM Higgs self-couplings via $HHH\nu\bar{\nu}$ production at future $e^-e^+$ colliders

Paula Martínez Suárez

Supervisor: M<sup>a</sup> José Herrero Solans

Master's thesis for the Master's Degree in Theoretical Physics,  
Elementary Particles and Cosmology

UNIVERSIDAD AUTÓNOMA DE MADRID  
INSTITUTO DE FÍSICA TEÓRICA IFT UAM-CSIC

September 2020





## Agradecimientos

Con este trabajo de fin de máster doy fin a mi etapa como estudiante, de la cual puedo enorgullecerme gracias a la contribución de muchas otras personas aparte de mí misma. En primer lugar, gracias a mis padres por apoyarme siempre en mis decisiones, incluso a pesar de las dificultades económicas, y motivarme para dedicarme a mi pasión. Gracias también a la Universidad de Oviedo y a su grupo de Física de Altas Energías, quienes me introdujeron por primera vez a la que acabaría siendo mi rama favorita de la Física, y gracias a los cuales pude disfrutar de uno de los mejores veranos de mi vida como parte de DESY. Gracias al máster de Física Teórica de la UAM, y en particular a María José Herrero, por inculcarme todos los conocimientos necesarios para la realización de este proyecto tanto dentro como fuera de su asignatura, y a José Miguel No por responder a todas mis dudas siempre con una sonrisa. Por último, gracias a Manuel González y a Claudia García, ya que su investigación previa ha sido uno de los pilares de este trabajo.



# Abstract

The Standard Model of particle physics can be regarded as a very successful theory, and over the last decades, its predictions have led to very relevant discoveries in the field. However, there are both experimental evidence and theoretical problems which makes us think that the theory is still incomplete in several aspects, including the Higgs sector. The aim of this work is to test the sensitivity of the process  $e^-e^+ \rightarrow HHH\nu\bar{\nu}$  to Beyond the Standard Model triple and quartic autointeractions of the Higgs boson. To do so, we will use the parametrization given by the Electroweak Chiral Lagrangian, an effective field theory based on Chiral Perturbation Theory which allows us to quantify possible deviations from the Standard Model in a model independent way. We will start by introducing the theoretical framework and motivate why it is the best choice for us. Then, we will characterize the  $W^-W^+ \rightarrow HHH$  subprocess and quantify the deviations induced by anomalous Higgs self-couplings. Next, we will repeat the same analysis for triple Higgs production in  $e^-e^+$  colliders. Finally, we will study the sensitivity of a particular collider to these anomalous couplings. The results regarding the  $e^-e^+ \rightarrow HHH\nu\bar{\nu}$  process presented here constitute an original contribution from this work, and the study of the sensitivity to the triple and quartic self-coupling that we propose is, to our knowledge, a novel study.



# Contents

<b>1</b>	<b>Introduction</b>	<b>1</b>
<b>2</b>	<b>BSM Higgs self-couplings in the EFT approach</b>	<b>6</b>
2.1	The Electroweak Chiral Lagrangian . . . . .	6
2.2	Linear vs. non-linear parametrizations . . . . .	12
2.3	Some comments on unitarity . . . . .	13
<b>3</b>	<b>Sensitivity to BSM Higgs self-couplings in <math>W^-W^+ \rightarrow HHH</math></b>	<b>15</b>
3.1	The SM prediction . . . . .	16
3.2	Deviations induced by BSM self-couplings . . . . .	18
<b>4</b>	<b>Testing the BSM Higgs self-couplings via triple Higgs production at <math>e^-e^+</math> colliders</b>	<b>24</b>
4.1	WWS in $e^-e^+$ colliders . . . . .	25
4.2	The effective $W$ approximation . . . . .	27
4.3	SM prediction and BSM deviations from anomalous self-couplings . . . . .	31
4.4	Sensitivity to Higgs BSM self-couplings at $\sqrt{s} = 3000$ GeV . . . . .	36
<b>5</b>	<b>Conclusions</b>	<b>50</b>
	<b>Appendix</b>	<b>53</b>
I	Diagrams contributing to $W^-W^+ \rightarrow HHH$ . . . . .	53
II	Analytic expression for the $W^-W^+ \rightarrow HHH$ amplitude . . . . .	54
III	Variable redefinition for VEGAS numerical integration . . . . .	56
IV	Diagrams contributing to $e^-e^+ \rightarrow HHH\nu_e\bar{\nu}_e$ . . . . .	58
	<b>References</b>	<b>60</b>



# 1 Introduction

The Standard Model of Particle Physics (SM) is a theory which was developed during the 20th century [1–4] and successfully explains many aspects about the nature and interactions of the fundamental particles that can be observed in high energy experiments. This model is a quantum field theory built from the (gauge) symmetry group  $SU(3)_C \times SU(2)_L \times U(1)_Y$ , where  $SU(3)_C$  describes the strong interactions and  $SU(2)_L \times U(1)_Y$  refers to the electroweak (EW) sector. The mediators of each interaction are the corresponding gauge bosons associated to each gauge group, while the rest of the particles are organized in three generations of fermions (which can be quarks or leptons, depending on their color charge) plus the Higgs boson, being the latter the main interest of this work.

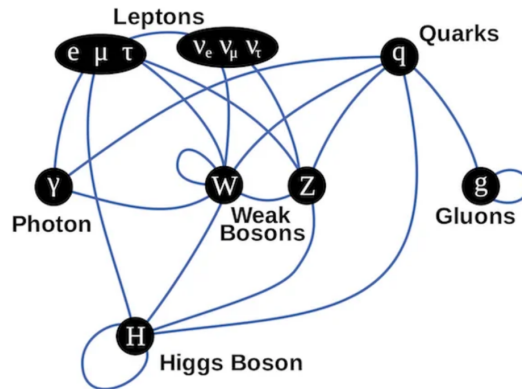


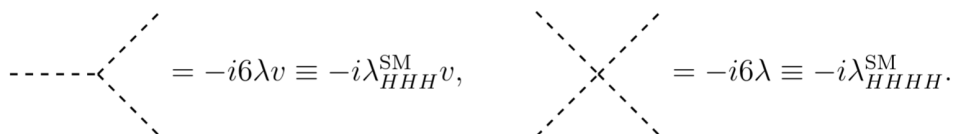
**Figure 1.1:** Particle content of the Standard Model and the corresponding interactions.

The Higgs boson is the only scalar (spin 0) particle in the SM. It is introduced in the model *a posteriori* to generate the masses of the fundamental particles (except for neutrinos) without breaking gauge invariance via the Brout-Englert-Higgs (BEH) mechanism [5–9]. According to Goldstone Theorem [10], if a quantum field theory has a global continuous symmetry which is not a symmetry of the vacuum (a symmetry is *spontaneously broken*), there has to be a massless boson (scalar or pseudoscalar) associated to each symmetry which does not leave the vacuum invariant. This is, for example, how pions are generated in QCD. When we consider the case in which the masses of the quarks are zero (which is a good approximation for up and down quarks), the Lagrangian is invariant under the  $SU(2)_L \times SU(2)_R$  global symmetry group, usually named the chiral symmetry, but the vacuum is only invariant under the diagonal  $SU(2)_{L+R}$  group. Since  $\dim[SU(2)_L \times SU(2)_R] - \dim[SU(2)_{L+R}] = 3$ , three Goldstone bosons appear, which are identified as the three pions ( $\pi^0$  and  $\pi^\pm$ ), whose masses are much smaller than the typical hadron masses ( $\gtrsim 1$  GeV vs.  $\sim 100$  MeV for pions). The only reason why  $m_\pi \neq 0$  is simply that the up and down quarks are not truly massless, and the global symmetry is explicitly broken (it is an approximate symmetry). This is the reason why pions are called *pseudo* Goldstone bosons.

However, when the broken symmetry is a gauge symmetry, the would-be Goldstone bosons associated to the breaking do not appear in the spectrum, but instead combine with the massless gauge vector bosons in such a way that they appear as massive particles in the spectrum that we build from the true vacuum. Based on this principle, the BEH mechanism introduces a new complex scalar field  $\Phi$  in the SM, which is a doublet of  $SU(2)_L$  charged under the symmetry groups that we need to break ( $T = 1/2$  and  $Y = 1$ ). Below a critical temperature (energy), this field acquires a vacuum expectation value (also called vev or simply  $v$ ) and the true vacuum is not invariant under  $SU(2)_L \times U(1)_Y$  anymore. The  $\Phi$  field is a complex doublet, and therefore it has four degrees of freedom. Three of them are absorbed by the  $W^\pm$  and  $Z$  gauge bosons, each of them acquiring a longitudinal degree of freedom and becoming massive, while the remaining one is the Higgs field  $H$ , which parametrizes the oscillations around the vacuum. Since the real scalar component of the field  $\Phi$  acquiring a vev is not electrically charged, the symmetry under the electromagnetic gauge group  $U(1)_{EM}$  is preserved and the mediator of the electromagnetic interactions, the photon, remains massless. After introducing the BEH mechanism and going to the unitary gauge, the scalar part of the SM Lagrangian,  $\mathcal{L}_H$ , reads:

$$\begin{aligned} \mathcal{L}_H = & - \sum_f \frac{m_f}{v} \bar{f} H f + 2m_W^2 W_\mu^+ W_\mu^- \left( \frac{H}{v} + \frac{H^2}{2v^2} \right) + m_Z^2 Z_\mu Z^\mu \left( \frac{H}{v} + \frac{H^2}{2v^2} \right) \\ & - \lambda v H^3 - \frac{1}{4} \lambda H^4, \end{aligned} \quad (1.1)$$

where  $\lambda = g^2 m_H^2 / 8m_W^2 = m_H^2 / 2v^2$ . From this Lagrangian we can obtain the corresponding Feynman rules, which we will use to define the triple and quartic Higgs self-couplings,  $\lambda_{HHH}$  and  $\lambda_{HHHH}$ :



$$\begin{aligned} \text{---} \text{---} \text{---} &= -i6\lambda v \equiv -i\lambda_{HHH}^{\text{SM}} v, & \text{---} \text{---} \text{---} \text{---} &= -i6\lambda \equiv -i\lambda_{HHHH}^{\text{SM}}. \end{aligned}$$

As we can see, the SM predicts the relation  $\lambda_{HHH}^{\text{SM}} = \lambda_{HHHH}^{\text{SM}}$ , so the measurement of the ratio between these two couplings is a direct test of the validity of the BEH mechanism, and would allow to determine if the assumption of  $\Phi$  being a doublet is correct, or if there is physics beyond the Standard Model (BSM) regarding the nature of the Higgs boson.

The BEH mechanism was theoretically developed in the 60s, although the  $W^\pm$  and  $Z$  bosons were not discovered until 1983 in the Super Proton-Antiproton Synchrotron (SppS) [11–14], with masses around 80 and 90 GeV, respectively, in agreement with the theoretical predictions. The confirmation of the existence of a Higgs boson took a couple of decades more, but it was finally discovered in 2012 in the Large Hadron Collider (LHC)

when the ATLAS and CMS collaborations announced the measurement of a scalar, neutral particle, with a mass around 125 GeV [15, 16] compatible with the theory. However, there are several facts that point that the SM is still incomplete. Some of them come from experimental evidence, such as the existence of dark matter or the fact that neutrinos are not massless. Others are theoretical issues regarding fine-tuning problems with some of the free parameters of the theory, for example, the flavour puzzle, the strong CP problem or the hierarchy problem, being the last one directly related to the Higgs boson and its mass.

The mass of the Higgs boson is a free parameter of the SM, and therefore can only be determined experimentally. This was done at the LHC, fixing the Higgs boson mass at 125 GeV. This mass is not protected by any symmetry, which means that no symmetry is restored when it is set to 0. Therefore, if the SM is taken as a low energy effective field theory valid up to a cutoff scale  $\Lambda^1$ , then the mass of the Higgs boson can receive large additive corrections proportional to the  $\Lambda$  scale, which are many orders of magnitude higher than the experimental value. As a consequence, reproducing the 125 GeV measured mass would require a huge fine-tuning in the bare mass. In order to solve this problem, two types of theories have been proposed. On the one hand, it may happen that the Higgs boson is an elementary particle. In that case, the hierarchy problem could be solved introducing new symmetries that protect the Higgs boson mass, as it is done, for instance, in supersymmetric theories. On the other hand, the Higgs boson could also be a composite state, a bound state from a new type of strong interaction. However, which theory is the correct one remains unclear, and the hierarchy problem is far from closed.

In the lack of a unique UV (high energy) theory, effective field theories (EFTs) have gained popularity, since they allow to study low energy effects of a new UV theory below a certain threshold without any specific information about the dynamics above that threshold. It is assumed that the possible new particles are too massive to propagate at the energies that are probed, so they can be integrated out from the theory. Nevertheless, they do not completely disappear, since their low energy effects can be measured as deviations from the SM. Furthermore, the new physics in EFTs is usually summarized by a collection of effective operators, built with the SM fields and ordered by their increasing dimension, which can be different from 4. The requirement on these effective operators is based just on the needed symmetries, including the SM gauge symmetry,  $SU(3)_C \times SU(2)_L \times U(1)_Y$ . The information on the new UV physics BSM is encoded then in the particular values of the coefficients in front of these effective operators. One of the simplest examples of an EFT is Fermi's theory of beta decay [17], which is a theory for weak interactions previous to the discovery of the  $W$  boson. In this formulation, processes mediated by a  $W$  boson are collapsed to an interaction point proportional to the Fermi

---

<sup>1</sup>It is expected that the SM is not valid at arbitrarily large energies.  $\Lambda$  can be, for example, the Planck scale,  $\Lambda_{\text{Planck}} \sim 10^{19}$  GeV, or the GUT scale,  $\Lambda_{\text{GUT}} \sim 10^{16}$  GeV.

coupling constant,  $G_F = \sqrt{2}g^2/8m_W^2$ , which contains the effect of the intermediate  $W$  boson that is integrated out at low energies. Here, we will use a similar technique to study possible deviations in the scalar sector of the SM, and in particular, in the Higgs boson self-couplings, based on the Electroweak Chiral Lagrangian (EChL, also called Higgs Effective Field Theory or HEFT). In this EFT approach the electroweak chiral symmetry of the scalar sector of the SM is realized non-linearly (like the chiral symmetry in QCD) and the Higgs particle is introduced as a singlet. This is in contrast to other EFTs like the SMEFT where the Higgs particle is introduced inside the  $\Phi$  doublet and the EW chiral symmetry is realized linearly. The feature that  $H$  is a singlet within the EChL approach allows us to consider the two BSM Higgs self-couplings,  $\lambda_{HHH}$  and  $\lambda_{HHHH}$ , as a priori uncorrelated, reason why the EChL is the proper EFT for our purpose in this work.

But the measurement of these couplings is not an easy task, because the processes that depend on these quantities involve multiple Higgs production. In the current LHC with proton-proton collisions at a center of mass energy of 13 TeV, the production cross section of two or more Higgs bosons is in the picobarn (pb) scale or below [18], and the luminosity is not high enough to produce good statistics. Nevertheless, the trilinear self-coupling has been constrained by the ATLAS Collaboration [19] to  $-2.3 < \lambda_{HHH}/\lambda_{HHH}^{\text{SM}} < 10.3$  at the 95% CL, being  $\lambda_{HHH}^{\text{SM}}$  the value in the SM, under the assumption that the new physics affects only the  $\lambda$  parameter. The quartic self-coupling by the moment remains inaccessible. A more precise determination of the trilinear self-coupling via double Higgs production is one of the aims of several future projects, such as the High Luminosity LHC (HL-LHC) and its high energy upgrade (HE-LHC) [20], the International Linear Collider (ILC) [21] and the Compact Linear Collider (CLIC) [22], and much research on this topic has already been done. The study of triple Higgs production as a way to test new couplings of the Higgs boson to SM particles has already been proposed for future proton-proton colliders at very high energies above 14 TeV such as, for example, the Future Circular Collider (FCC) [23, 24]. In this work we will focus on the two electron-positron colliders in the list: the ILC and CLIC. They will operate in several stages with different values of the center of mass energy and different integrated luminosities, as it can be seen in the following table:

Collider	$\sqrt{s}$ (GeV)	$\mathcal{L}_{\text{int}}$ ( $\text{ab}^{-1}$ )
ILC	250	2
	350	0.2
	500	4
	1000	8
CLIC	380	1
	1500	2.5
	3000	5

**Table 1.1:** Expected center of mass energies and integrated luminosities in the different stages of both the ILC and CLIC. The beams are assumed to be unpolarized, although modifications in the polarization can lead to an enhancement of a particular signal.

While the low energy stages are optimized to measure the Yukawa couplings to other particles, the high energy stages are designed for a more precise measurement of the trilinear self-coupling,  $\lambda_{HHH}$  through double Higgs production. Throughout this work we will argue that under certain conditions it could also be possible for this type of collider to study triple Higgs production, which can provide additional information about the trilinear self-coupling  $\lambda_{HHH}$  and, in some cases, even the quartic self-coupling  $\lambda_{HHHH}$ . To study the sensitivity to these couplings in such colliders, we will focus on  $WW$  scattering (WWS), the dominant production mechanism for double and triple Higgs at high energies. This process, apart from exhibiting the highest cross section, is also interesting because any deviation from the SM in the self-couplings leads to an increase in the production rate, something that does not happen in other important production mechanisms, such as associated production with a  $Z$  boson. Furthermore, it is a purely electroweak tree-level process (the dominant production mechanism in a proton-proton collider is gluon fusion, which involves quark loops and the top Yukawa coupling) and has a clean experimental signal, with missing transverse momentum and two(three) Higgs bosons, which will mainly decay to bottom quarks and produce four(six) b-jets. Since in an  $e^-e^+$  collider the initial particles (electrons and positrons) are fundamental, these type of signals should be easier to filter than in a proton-proton collider, where the hadronic character of the protons leads to huge QCD backgrounds. In summary, we will study multiple Higgs production via WWS at future  $e^-e^+$  colliders to see if it would be possible to measure BSM deviations of the Higgs self-couplings also via triple Higgs production, which, unlike double Higgs production, could also provide information about the quartic self-coupling.

This work is organized as follows: in Section 2 we will introduce the EChL and its phenomenological implications. In Section 3 we will analyze the  $W^-W^+ \rightarrow HHH$  subprocess in detail, both in the SM and beyond, and see how sensitive it is to variations of the Higgs boson self-couplings. In Section 4, the corresponding results for  $e^-e^+$  collisions will be presented, together with an estimation of the number of events that (if possible)

could be detected in a real collider in the most favorable case. The conclusions are summarized in Section 5. The contents of Sections 4 and 5 show the original research work of this master's thesis. All the computations, plots, results and conclusions on the sensitivity to the BSM Higgs self-couplings are original contributions of this work. In particular, the study of the sensitivity to the quartic self-coupling presented here is, to our knowledge, a novel study.

## 2 BSM Higgs self-couplings in the EFT approach

As we mentioned in the previous section, the BEH mechanism allows to generate the masses of the fundamental particles without breaking gauge invariance, and the resulting predictions have led to very important discoveries in the field. However, the true nature of the Higgs boson is still unclear, reason why it is interesting to study the symmetry breaking using an effective theory. When writing an EFT for the EW symmetry breaking sector (SBS), different parametrizations of the fields can be used depending on the underlying physics that we are interested in. As we will see, all of them are based on the global  $SU(2)_L \times SU(2)_R$  symmetry of the SBS and the EW  $SU(2)_L \times U(1)_Y$  gauge symmetry of the SM, but the choice between one or another may seem more natural, for example, depending on whether the underlying physics is weakly- or strongly-coupled. In this section we will try to motivate why the EChL is a good option for our study.

### 2.1 The Electroweak Chiral Lagrangian

Chiral Lagrangians were first employed in Quantum Chromodynamics (QCD) [25], taking their name from the global  $SU(2)_L \times SU(2)_R$  symmetry (the chiral symmetry) that explains the existence of three very light mesons (the pions) as pseudo Goldstone bosons which appear when the symmetry is spontaneously broken. The QCD Chiral Lagrangian is an EFT for QCD which describes pion dynamics below the GeV scale, integrating out the rest of heavier particles and ignoring their composite nature. Electroweak Chiral Lagrangians, first developed in the 80s [26–30], follow the same idea, applied to the Goldstone bosons (GB) that arise from EWSSB and mix with the  $W^\pm$  and  $Z$  gauge bosons. Using the EChL we can study the GB dynamics and how they couple to the Higgs boson.

To see how we can build the EChL, let's start by examining the SBS of the SM in more detail. As we explained in the previous section, the BEH mechanism allows to generate the masses of the EW gauge bosons by introducing a complex scalar doublet  $\Phi$ , which is defined as:

$$\Phi = \begin{pmatrix} \phi^+ \\ \phi^0 \end{pmatrix}. \quad (2.1)$$

Since the components take complex values, the field has four degrees of freedom. The dynamics of this field are described by the following Lagrangian (for the purpose of this work we will ignore the interactions with fermions):

$$\mathcal{L}_{\text{SBS}} = (D_\mu \Phi)^\dagger (D^\mu \Phi) + \mu^2 (\Phi^\dagger \Phi) - \lambda (\Phi^\dagger \Phi)^2 \equiv (D_\mu \Phi)^\dagger (D^\mu \Phi) - V(\Phi), \quad (2.2)$$

where  $D_\mu \Phi$  refers to the covariant derivative:

$$D_\mu \Phi = \left( \partial_\mu - \frac{ig}{2} \vec{W}_\mu \cdot \vec{\tau} - \frac{ig'}{2} B_\mu \right) \Phi. \quad (2.3)$$

Here  $\vec{W}_\mu = (W_\mu^1, W_\mu^2, W_\mu^3)$  and  $B_\mu$  are the three gauge boson mediators associated to the  $\text{SU}(2)_L$  group and the mediator associated to the  $\text{U}(1)_Y$  group, respectively. The respective gauge couplings are  $g = e/\sin \theta_w$ ,  $g' = e/\cos \theta_w$  (being  $\theta_w$  the weak mixing angle) and  $\vec{\tau} = (\tau^1, \tau^2, \tau^3)$  are the Pauli matrices.

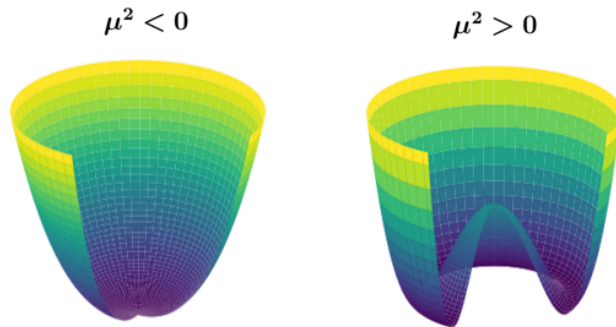


**Figure 2.1:** Qualitative representation of the potential  $V(\Phi)$  in the symmetric phase (left) and in the broken phase (right).

The Lagrangian in equation 2.2 is  $\text{SU}(2)_L \times \text{U}(1)_Y$  gauge invariant, but the vacuum can respect the symmetry or not, depending on the value of  $\mu^2$ . As it is shown in figure 2.1, when  $\mu^2 < 0$  the potential has a single minimum, which corresponds to  $\langle 0|\Phi|0\rangle = 0$ ; in this case, the symmetry is not spontaneously broken. However, when  $\mu^2 > 0$  the field acquires a vacuum expectation value  $v$  and the true minimum becomes degenerate around a circumference of fixed radius in the complex plane:

$$|\langle 0|\Phi|0\rangle| = \frac{1}{\sqrt{2}} \begin{pmatrix} 0 \\ v \end{pmatrix}, \quad (2.4)$$

where  $v = \sqrt{\mu^2/\lambda}$ . The choice of one of these vacua is what causes the breaking of the

$SU(2)_L \times U(1)_Y$  symmetry to  $U(1)_{EM}$ . To see how this mechanism generates masses for the gauge bosons, we can choose one vacuum (for example,  $\langle 0|\Phi|0\rangle = |\langle 0|\Phi|0\rangle|$ ) and then study the (small) oscillations of the field around it. To do so, we parametrize the  $\Phi$  field in polar coordinates, where  $H$  refers to the radial direction and  $\vec{\xi} = (\xi^1, \xi^2, \xi^3)$  to the angular direction:

$$\Phi = \frac{1}{\sqrt{2}} \begin{pmatrix} 0 \\ v + H \end{pmatrix} \exp\left(\frac{i\vec{\xi} \cdot \vec{\tau}}{v}\right). \quad (2.5)$$

The  $\vec{\xi}$  fields are the so-called would-be Goldstone bosons, and there is one for each broken generator of the symmetry. These fields are not physical, but they can be removed performing a gauge transformation (going to the *unitary gauge*):

$$\Phi \rightarrow U(\xi)\Phi = \frac{1}{\sqrt{2}} \begin{pmatrix} 0 \\ v + H \end{pmatrix}. \quad (2.6)$$

The  $\vec{W}_\mu$  and  $B_\mu$  fields that appear in the derivative term of  $\mathcal{L}_{SBS}$  are the EW eigenstates and transform as:

$$\begin{aligned} \frac{1}{2}\vec{W}_\mu \cdot \vec{\tau} &\rightarrow \frac{1}{2}\vec{W}'_\mu \cdot \vec{\tau} = U(\xi) \left( \frac{1}{2}\vec{W}_\mu \cdot \vec{\tau} \right) U^{-1}(\xi) - \frac{i}{g} [\partial_\mu U(\xi)] U^{-1}(\xi), \\ B_\mu &\rightarrow B'_\mu = B_\mu, \end{aligned} \quad (2.7)$$

and allow us to define the *mass eigenstates*  $W_\mu^\pm$ ,  $Z_\mu$  and  $A_\mu$ :

$$\begin{aligned} W_\mu^\pm &= \frac{1}{\sqrt{2}}(W_\mu'^1 \mp iW_\mu'^2), \\ Z_\mu &= \cos\theta_w W_\mu'^3 - \sin\theta_w B'_\mu, \\ A_\mu &= \sin\theta_w W_\mu'^3 + \cos\theta_w B'_\mu. \end{aligned} \quad (2.8)$$

After applying all these changes to 2.2, the derivative part yields the kinetic term for the  $H$  field and mass terms for the  $W^\pm$  and  $Z$  bosons (the  $A_\mu$  field, which corresponds to the photon, remains massless):

$$(D_\mu \Phi)^\dagger (D^\mu \Phi) = \frac{1}{2}(\partial_\mu H)(\partial^\mu H) + m_W^2 W_\mu^+ W_\mu^- + \frac{1}{2}m_Z^2 Z_\mu Z^\mu + \dots \quad (2.9)$$

where:

$$m_W = \frac{gv}{2}, \quad m_Z = \frac{\sqrt{g^2 + g'^2}v}{2}, \quad (2.10)$$

while the potential term contains the mass term and the self-interactions of the Higgs

boson:

$$-V(\Phi) = \mu^2(\Phi^\dagger\Phi) - \lambda(\Phi^\dagger\Phi)^2 = -\frac{1}{2}m_H^2 H^2 - \lambda v H^3 - \frac{1}{4}\lambda H^4, \quad (2.11)$$

where  $m_H = \sqrt{2\mu^2}$ .

The value of the vacuum expectation value  $v$  can be obtained from the connection of the SM EW Lagrangian with the preceding Fermi effective theory, which establishes a relation between the Fermi constant  $G_F$  and  $v$ :

$$G_F = \frac{1}{\sqrt{2}v^2} \quad \rightarrow \quad v \simeq 246 \text{ GeV}. \quad (2.12)$$

Apart from being responsible for the generation of the EW boson masses (and indirectly, fermion masses), the fact that the Higgs field  $H$  is embedded in a doublet also induces correlations between the different couplings. These correlations are responsible for the cancellation of the divergent behaviour of longitudinal boson scattering at high energies and unitarity restoring, and fix the self-couplings of three and four  $H$  to be related via  $v$ , as it can be seen in equation 2.11. Nevertheless, we can relax these conditions if our purpose is to study the SM from an effective approach because, on the one hand, preserving unitarity at all energies is not a necessary condition for an EFT to be valid, since the theory itself may not be valid at all energy scales. In this case unitarity violation would give an upper bound at which the EFT breaks and new UV physics is required. On the other hand, the Higgs self-couplings are poorly constrained by the experiment due to the low cross sections of the processes that allow to study them, so it is not discarded that they (and in particular, their ratio) can differ from the SM prediction in a significant amount. In summary, we are now interested in an EFT that does not necessarily preserve unitarity at all scales but allows us to vary the Higgs self-couplings independently and see how these variations modify the corresponding cross sections. To this purpose we introduce the EChL.

Let's start by rewriting the SBS Lagrangian of the SM in terms of a new matrix  $M$ , defined as:

$$M \equiv (\tilde{\Phi}\Phi) = \begin{pmatrix} \phi_0^* & \phi^+ \\ -\phi^- & \phi^0 \end{pmatrix} \quad \text{where} \quad \tilde{\Phi} = i\tau^2\Phi^* = \begin{pmatrix} \phi_0^* \\ -\phi^- \end{pmatrix}. \quad (2.13)$$

Then:

$$\begin{aligned} \mathcal{L}_{\text{SBS}} &= \frac{1}{2}\text{Tr}[(D_\mu M)^\dagger(D^\mu M)] - V(M) \\ V(M) &= -\frac{1}{4}\lambda \left( \text{Tr}(M^\dagger M) + \frac{\mu^2}{\lambda} \right)^2, \end{aligned} \quad (2.14)$$

with the covariant derivative now defined as:

$$D_\mu M = \partial_\mu M + \frac{ig}{2}(\vec{W}_\mu \cdot \vec{\tau})M - \frac{ig'}{2}B_\mu M\tau^3, \quad (2.15)$$

to match the one in 2.3. Introducing the matrix  $M$  makes the  $SU(2)_L \times SU(2)_R$  symmetry (the EW chiral symmetry) of the SBS explicit, since we can now easily see that the Lagrangian is invariant under global transformations of the type:

$$M \rightarrow LMR^\dagger,$$

where  $L \in SU(2)_L$  and  $R \in SU(2)_R$ . When  $\Phi$  acquires a vacuum expectation value this symmetry is spontaneously broken to  $SU(2)_{L+R}$ . The situation is very similar to QCD, with the difference that in this case the  $SU(2)_L$  group and (only) the  $U(1)_Y$  subgroup of  $SU(2)_R$  are gauged, leading to different physical consequences when the symmetry breaks. Electroweak Chiral Lagrangians are based on this EW chiral symmetry and its breaking to  $SU(2)_{L+R}$ , but using a non-linear representation, which means that the three Goldstone bosons  $\xi^1, \xi^2, \xi^3$  transform non-linearly under the global  $SU(2)_L \times SU(2)_R$ . The Higgs boson is in this case introduced as a *singlet* under the EW chiral symmetry, independent from the Goldstone bosons, which are all included in an exponential representation. For our purposes it is enough to use the leading order EChL [31, 32], which reads:

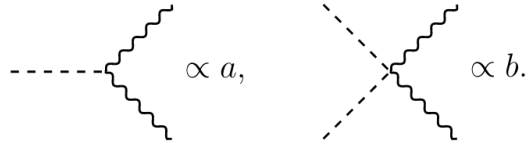
$$\begin{aligned} \mathcal{L}_{\text{EChL}} = & \frac{v^2}{4} \left[ 1 + 2a \left( \frac{H}{v} \right) + b \left( \frac{H}{v} \right)^2 + \dots \right] \text{Tr}[D_\mu U^\dagger D^\mu U] + \frac{1}{2}(\partial_\mu H)(\partial^\mu H) \\ & - \frac{1}{2}m_H^2 H^2 - \kappa_3 \lambda v H^3 - \kappa_4 \frac{1}{4} \lambda H^4 + \dots \end{aligned} \quad (2.16)$$

where  $U$  is the  $2 \times 2$  matrix that contains the Goldstone bosons:

$$U \equiv \exp \left( \frac{i\vec{\xi} \cdot \vec{\tau}}{v} \right), \quad (2.17)$$

and  $H$  is a singlet under  $SU(2)_L \times U(1)_Y$ , so it enters the EChL via polynomial functions. As in any other EFT whose low energy limit is the SM, the information of the new UV physics which is assumed to be integrated out is encoded in the values of the effective Lagrangian parameters. In equation 2.16 these are  $a$ ,  $b$ ,  $\kappa_3$  and  $\kappa_4$  (although additional parameters can be introduced).

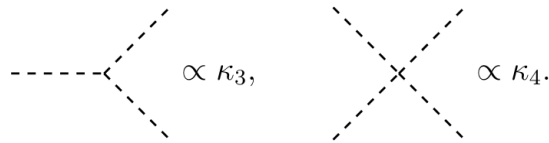
In this Lagrangian, the parameters  $a$  and  $b$  control the so-called anomalous couplings of the Higgs boson to  $W$  and  $Z$  bosons as follows:



The SM couplings are recovered when  $a = b = 1$ . Both parameters have been constrained by one or more methods. For example, the ATLAS Collaboration has set the following bounds on each of them using single and double Higgs production:

$$a \in [0.97, 1.13] \quad [33] \quad b \in [-0.76, 2.90] \quad [34] \quad (2.18)$$

On the other hand, the parameters  $\kappa_4$  and  $\kappa_3$  control the triple and quartic Higgs self couplings, that is:



Again, the SM couplings correspond to  $\kappa_3 = \kappa_4 = 1$ . Although the value of  $\kappa_3$  can also be extracted from double Higgs production at the LHC, the sensitivity is lower, which leads to the bound that we already mentioned, much less restrictive than the ones for  $a$  and  $b$ :

$$\kappa_3 \in [-2.3, 10.3] \quad [19] \quad (2.19)$$

Here we would like to emphasize that currently there are no bounds for  $\kappa_4$ .

It is important to note that all these bounds are not completely general; they can depend on the underlying theory that it is assumed to interpret the results. For example, constraints on  $\kappa_3$  can be less restrictive if we allow deviations in the top Yukawa coupling, which is also involved in the analysis that yields the limits that we have just shown. In this work we will only consider deviations in the  $\kappa_3$  and  $\kappa_4$  parameters, and will assume that any other coupling takes its SM value. In particular, we will explore anomalous Higgs self-couplings by varying  $\kappa_3$  and  $\kappa_4$  in the range:

$$\kappa_3 \in [-10, 10] \quad \kappa_4 \in [-10, 10]. \quad (2.20)$$

With this choice we will be safe from unitarity violation (as we will check later), but stronger deviations could be allowed too.

## 2.2 Linear vs. non-linear parametrizations

The EChL is a non-linear EFT since the Goldstone bosons are introduced in exponential form and transform non-linearly under the symmetry group. But as we said before, it is not the only possible representation. In fact, observables are independent of the representation that we choose. One very common representation apart from the non-linear description is the linear one. The Standard Model Effective Field Theory (SMEFT) [35, 36] is an example of a linear model which introduces higher dimensional operators built from the SM fields that respect the  $SU(3)_C \times SU(2)_L \times U(1)_Y$  gauge symmetry. In this representation the Goldstone bosons are defined within a scalar doublet, along with the Higgs boson, as it is done in the SM. The deviations in this model come from new particles whose masses are of the same order as the cutoff scale  $\Lambda$ , which are assumed to be out of the experimental reach. Following this prescription, the SMEFT lagrangian is defined in its most generic form<sup>2</sup> as:

$$\mathcal{L}_{\text{SMEFT}} = \mathcal{L}_{\text{SM}} + \mathcal{L}^{(5)} + \mathcal{L}^{(6)} + \mathcal{L}^{(7)} + \mathcal{L}^{(8)} + \dots \quad (2.21)$$

where  $\mathcal{L}_{\text{SM}}$  is the SM lagrangian and:

$$\mathcal{L}^{(d)} = \sum_{i=1}^{n_d} \frac{C_i^{(d)}}{\Lambda^{d-4}} Q_i^{(d)} \quad (2.22)$$

contains the dimension  $d$  operators  $Q_i^{(d)}$  that respect the required symmetries, multiplied by the corresponding Wilson coefficients  $C_i^{(d)}$ . They are suppressed by  $d - 4$  powers of the cutoff scale.

The main difference between this type of EFTs and the EChL lies on the dimensional counting used to sort the different terms. In the case of a linear theory, the sorting is done according to the canonical dimension of the operators. Higher order operators have a higher dimension, which is compensated by an inverse power of the cutoff scale so all the terms have dimension four. In the case of the chiral lagrangian, the operator  $U$  which contains the Goldstone fields is adimensional, so a different prescription is used for the expansion, the chiral dimensional counting [37, 38], which means that a term  $\mathcal{L}_d$  with “chiral dimension”  $d$  will contribute to  $\mathcal{O}(p^d)$  in the corresponding power momentum expansion.

If we are working with a linear theory, the Higgs boson is embedded in a complex doublet  $\Phi$ . This means that a) to study triple and quartic interactions of the field we need to go

---

<sup>2</sup>Odd-dimension operators are usually neglected since they violate lepton number conservation ( $d = 5$ ) or  $B - L$  invariance ( $d \geq 7$ ), which are constrained to be extremely small.

at least<sup>3</sup> to terms of  $\mathcal{O}[(\Phi^\dagger\Phi)^2]$ , but terms of higher order can also contain dependences in  $h^3$  or  $h^4$  and b) due to the doublet nature of  $\Phi$ , the two couplings corresponding to  $h^3$  and  $h^4$  will then appear correlated. Because the EChL contains all the information about the  $h^3$  and  $h^4$  interactions in a polynomial expansion, the two lowest order terms already contain all the physics relating the couplings that we want to study, and they are completely independent from each other. This is mainly the reason why we choose to parametrize the BSM Higgs self-couplings using the EChL.

### 2.3 Some comments on unitarity

Throughout this section we have repeatedly mentioned that unitarity should not be violated in order to use a given theory to interpret the experimental results, but what exactly is unitarity? When we talk about unitarity, we are actually referring to the unitarity of the  $S$  matrix, which is the operator that relates the initial and the final state of the system. When the particles involved in the process do not interact at all, the  $S$  matrix is simply the unity; in general, it takes the form:

$$S = 1 + iT. \quad (2.23)$$

This expression has two parts, since even in an interacting theory there is the possibility that the particles do interact ( $T$  matrix) or miss one another and do not interact at all (identity matrix).

The requirement for this matrix to be unitary means nothing else than imposing that the probability of a process to happen does not exceed the unity. This constrain can be translated to a condition over the transition amplitude,  $T$

$$S^\dagger S = SS^\dagger = 1 \quad \rightarrow \quad (T - T^\dagger) = iT^\dagger T \quad \rightarrow \quad 2\text{Im}(T) = |T|^2, \quad (2.24)$$

In a  $2 \rightarrow 2$  process, this condition can be written in terms of *partial waves*. The method consists on expanding the scattering amplitudes in a new basis and apply the constraints coming from  $T$ . For instance, if we have a process  $1, 2 \rightarrow 3, 4$  the amplitude for a fixed initial and final polarization state can be written as:

$$\mathcal{M}_{\lambda_1\lambda_2\lambda_3\lambda_4}(s, \cos\theta) = 16\pi K \sum_J (2J+1) D_{\lambda\lambda'}^J(\cos\theta) a_{\lambda_1\lambda_2\lambda_3\lambda_4}^J(s), \quad (2.25)$$

where  $D_{\lambda\lambda'}^J$  are the Wigner functions,  $\lambda = \lambda_1 - \lambda_2$  and  $\lambda' = \lambda_3 - \lambda_4$  and  $K$  takes the value 1 or 2 depending on whether the final state particles are distinguishable or not.

---

<sup>3</sup>Terms of  $\mathcal{O}(\Phi^3)$  should not appear due to the requirement of hermiticity of the Lagrangian.

$a_{\lambda_1\lambda_2\lambda_3\lambda_4}^J(s)$  is the amplitude of the  $J$ -th partial wave, which can be calculated as:

$$a_{\lambda_1\lambda_2\lambda_3\lambda_4}^J(s) = \frac{1}{32\pi K} \int_{-1}^1 d\cos\theta D_{\lambda\lambda'}^J(\cos\theta) \mathcal{M}_{\lambda_1\lambda_2\lambda_3\lambda_4}(s, \cos\theta) \quad (2.26)$$

If we now write the condition in 2.24 in terms of these partial wave amplitudes, we obtain the following equation:

$$\text{Im}[a_{\lambda_1\lambda_2\lambda_3\lambda_4}^J(s)] = \Gamma(s, m_i) |a_{\lambda_1\lambda_2\lambda_3\lambda_4}^J(s)|^2. \quad (2.27)$$

where  $\Gamma(s, m_i)$  accounts for the factor coming from phase space integration, and is approximately one when  $s \gg m_i^2$ , i.e. at very high energies. In that case equation 2.27 yields the simpler condition:

$$|a_{\lambda_1\lambda_2\lambda_3\lambda_4}^J(s)| \leq 1, \quad (2.28)$$

which must be fulfilled in order to preserve unitarity.

This is a useful method to study unitarity limits in processes such as double Higgs production. The main goal of this work is to provide novel results for  $HHH$  production; however, we will also show predictions for  $HH$  production, which can also be found in the literature, but we find interesting to reproduce here for an illustrative comparison with the  $HHH$  case. In particular, we will rely on previous works [39] regarding the  $WW \rightarrow HH$  subprocess and its unitarity constraints coming from deviations in the triple Higgs self-coupling.

If we now want to study the unitarity bounds for a  $2 \rightarrow n$  process, we can not use the same expansion directly, since our amplitude depends on a higher number of variables. Following references [40, 41], one way of introducing the partial wave amplitudes is to insert a complete set of intermediate states into its left-hand side, separating the elastic and the inelastic part:

$$2\text{Im}[T_{\text{el}}(2 \rightarrow 2)] = \int_{\Pi_2} |T_{\text{el}}(2 \rightarrow 2)|^2 + \sum_n \int_{\Pi_n} |T_{\text{inel}}(2 \rightarrow n)|^2.$$

Here  $\Pi_n$  refers to the  $n$ -body phase space. In this case, the following bound for  $\sigma_{\text{inel}}(2 \rightarrow n)$  is obtained after introducing the partial wave expansion for  $T_{\text{el}}(2 \rightarrow 2)$ :

$$\sigma_{\text{inel}}(2 \rightarrow n) \leq \frac{4\pi}{s} \quad (2.29)$$

This is the constraint that we will impose in the next section to check the unitarity of our predictions for  $\sigma(W^-W^+ \rightarrow HHH)$ . We anticipate here that all our predictions for

BSM physics coming from deviations in  $\kappa_3$  and  $\kappa_4$  are fully unitary for all the energies considered in this work.

### 3 Sensitivity to BSM Higgs self-couplings in $W^-W^+ \rightarrow HHH$

As we will show in the following section, the WWS production mechanism is our preferred process to study deviations in the Higgs self-couplings at high energies because it exhibits the higher cross section and the most pronounced enhancement in a BSM scenario. In an  $e^-e^+$  collider, this process can be seen as the interaction of two  $W$  bosons which are radiated by the electron and the positron, producing an electron neutrino and an electron antineutrino plus the result of the interaction of the two  $W$ 's. Therefore we can make a distinction between the process, which we will define as all the possible interactions that starting at the initial state  $e^-e^+$  produce the final state that we are looking for, and the subprocess, which in this case will refer to the interaction between the two  $W$  bosons that are radiated by the electron and the positron when they interact via WWS.

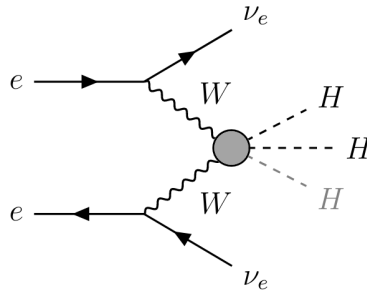


**Figure 3.1:** Multiple Higgs production via WWS.

For that reason, we will dedicate this section to characterize the  $W^-W^+ \rightarrow HHH$  subprocess within the SM and beyond, and compare the results with the better known  $W^-W^+ \rightarrow HH$ . Since the number of diagrams is considerably larger than in the two Higgs case, the generation of diagrams and their corresponding amplitudes will be done using FEYNARTS-3.10 [42] and FORMCALC-9.6 [43], while the phase space integration will be performed numerically using the VEGAS algorithm [44] implemented in Python. The obtained results have been checked using MADGRAPH 5 [45].

The diagrams used in the calculation of the cross section of the subprocess are shown in Appendix I, while the resulting analytic amplitude can be seen in Appendix II. In both this and the next section we will implicitly apply a set of changes of variables to perform the integration using VEGAS; the procedure is similar in both cases, and it is explained in detail in Appendix III.

### 3.1 The SM prediction

To compute the cross section for  $W^-W^+ \rightarrow HHH$  we can use the following equation for the differential cross section of a  $2 \rightarrow 3$  process:

$$d\sigma(1, 2 \rightarrow 3, 4, 5) = \frac{|\overline{\mathcal{M}}|^2}{4\sqrt{(p_1 \cdot p_2)^2 - m_1^2 m_2^2}} d\Pi_3(p_1 + p_2), \quad (3.1)$$

with  $1, 2 = W$  and  $3, 4, 5 = H$ . In this formula,  $|\overline{\mathcal{M}}|^2$  is the squared amplitude of the process averaged over initial states and summed over final states, and  $d\Pi_3$  the 3-body Lorentz invariant phase space (LIPS). To simplify the computation, we will calculate the cross section in the center of mass (CM) frame, defining the CM energy squared  $\hat{s} = (p_1 + p_2)^2 = (E_1 + E_2)^2$  and taking  $\vec{p}_1 + \vec{p}_2 = 0$ . Under this condition, the LIPS can be written as:

$$d\Pi_3(\sqrt{\hat{s}}, 0) = \frac{1}{32(2\pi)^4 \hat{s}} \int dm_{34}^2 dm_{45}^2 d\cos\theta_3 d\phi_{35}, \quad (3.2)$$

where  $m_{ij}^2 \equiv (p_i + p_j)^2$ ,  $\theta_3$  is the polar angle of particle 3 with respect to the  $z$  axis and  $\phi_{35}$  is the azimuthal angle of particle 5 with respect to particle 3. The integration limits for each variable are:

$$\begin{aligned} m_{34}^2 &\in [(2m_H)^2, (\sqrt{\hat{s}} - m_H)^2], & m_{45}^2 &\in [m_{45,\min}^2(m_{34}^2), m_{45,\max}^2(m_{34}^2)], \\ \cos\theta_3 &\in [-1, 1], & \phi_{35} &\in [0, 2\pi], \end{aligned} \quad (3.3)$$

with:

$$\begin{aligned} m_{45,\min}^2(m_{34}^2) &= (E_4^* + E_5^*)^2 - \left( \sqrt{E_4^{*2} - m_H^2} + \sqrt{E_5^{*2} - m_H^2} \right)^2, \\ m_{45,\max}^2(m_{34}^2) &= (E_4^* + E_5^*)^2 - \left( \sqrt{E_4^{*2} - m_H^2} - \sqrt{E_5^{*2} - m_H^2} \right)^2. \end{aligned} \quad (3.4)$$

$E_4^*$  and  $E_5^*$  are the energies of particles 4 and 5 in the rest frame of  $m_{34}^2$  ( $\vec{p}_3 + \vec{p}_4 = 0$ ) and can be written in terms of  $m_{34}^2$  as:

$$E_4^* = \frac{m_{34}}{2}, \quad E_5^* = \frac{1}{2m_{34}}(\hat{s} - m_{34}^2 - m_H^2). \quad (3.5)$$

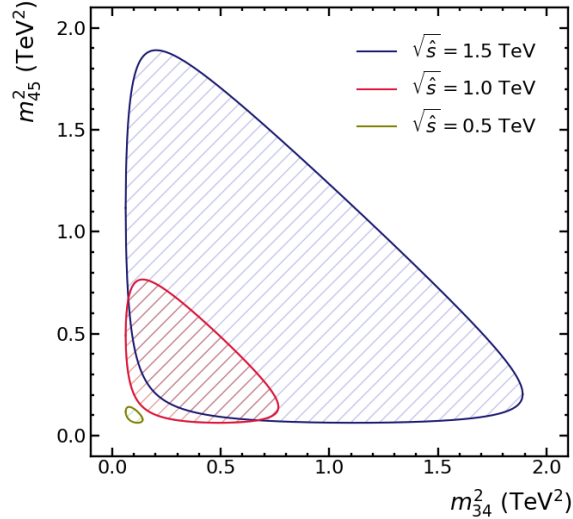


**Figure 3.2:** There exists a correlation between the values of  $m_{34}^2$  and  $m_{45}^2$ , as it can be seen in the so-called Dalitz plot. The shape of the integration region depends on the CM energy,  $\sqrt{\hat{s}}$ , and the mass of the final state particles 3, 4 and 5, which is  $m_H$  in our case.

After performing all the substitutions in 3.1, the result is:

$$\hat{\sigma}(W^-W^+ \rightarrow HHH) = \frac{1}{3!} \frac{1}{2\sqrt{\hat{s}^2 - 4\hat{s}m_W^2}} \frac{1}{32(2\pi)^4\hat{s}} \int dm_{34}^2 dm_{45}^2 d\cos\theta_3 d\phi_{35} |\overline{\mathcal{M}}|^2, \quad (3.6)$$

where the factor of  $1/3!$  is added due to the three identical particles in the final state.

This is the total (unpolarized) cross section, but it is also possible to compute the polarized cross section for a particular configuration of the initial  $W$  bosons. Assuming that they are both on-shell, each of them has three possible polarization states: longitudinal (L), transverse left (TL) and transverse right (TR). According to this, we define three possible initial states for the  $WW$  pair, LL (both longitudinal), LT+TL (one transverse and one longitudinal) and TT (both transverse). For each case we have a different factor in the average over initial states, being  $1/9$  for the unpolarized cross section,  $1$  for LL,  $1/2$  for LT+TL and  $1/4$  for TT. Plotting the results we can see (figures 3.3 and 3.4) how the LL configuration is clearly dominant in both double and triple Higgs production. One of the most interesting features is the fact that  $\sigma_{LL}$  is flat with  $\sqrt{\hat{s}}$  in  $HH$  production, but it increases with  $\sqrt{\hat{s}}$  in  $HHH$  production, so the latter is more sensitive to potential unitarity violation from BSM physics at high energies. While comparing the two cases,  $HH$  and  $HHH$  production, we also notice in figures 3.3 and 3.4 that the relative size of LT+TL is interchanged with respect to TT, being the TT contribution in  $HHH$  clearly well below the others.

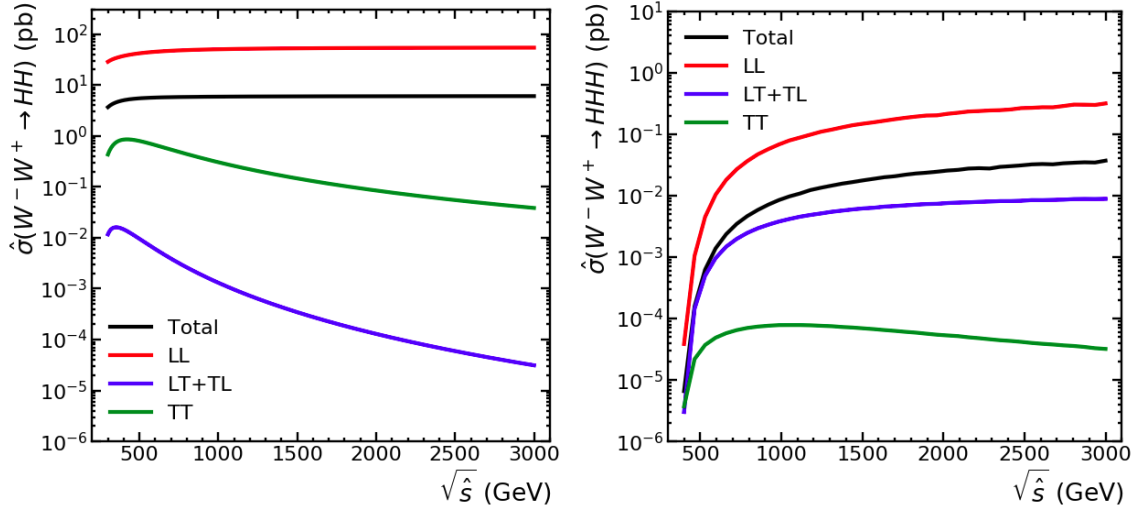


**Figure 3.3:** Polarized and total cross sections of the subprocess  $W^-W^+ \rightarrow HH$  (left) and  $W^-W^+ \rightarrow HHH$  (right) as a function of the CM energy  $\sqrt{\hat{s}}$ . The LL configuration is dominant in both cases, being this effect more significant in triple Higgs production.

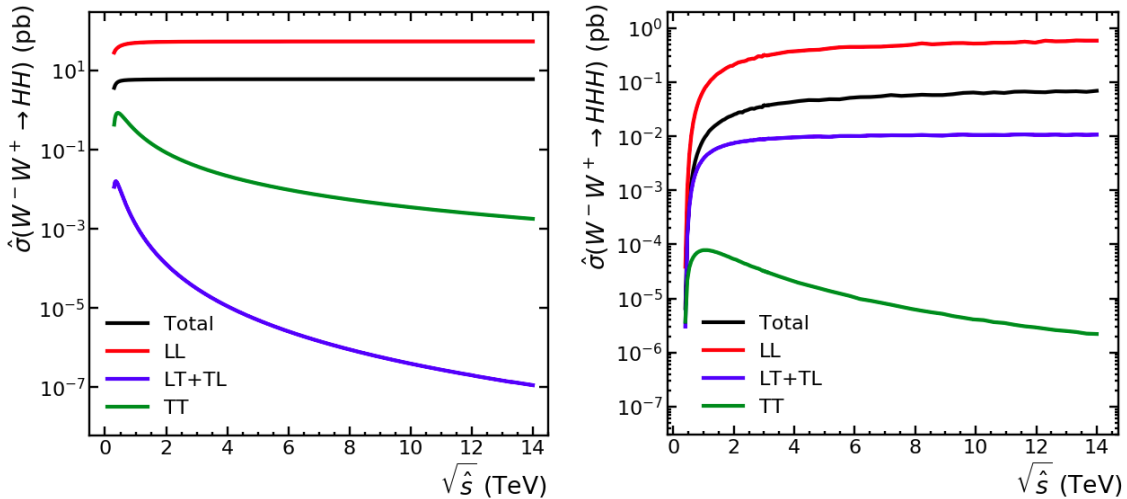


**Figure 3.4:** Figure 3.3 extended to  $\sqrt{\hat{s}} = 14$  TeV.

### 3.2 Deviations induced by BSM self-couplings

To study the deviations caused by BSM Higgs self-couplings, we define the new vertices in terms of  $\kappa_3$  and  $\kappa_4$  as:

$$\begin{array}{c} \text{---} \\ \text{---} \end{array} \begin{array}{c} \diagup \\ \diagdown \end{array} = -i\lambda_{HHH}v \equiv -i\kappa_3\lambda_{HHH}^{\text{SM}}v, \quad \begin{array}{c} \diagup \\ \diagdown \end{array} \begin{array}{c} \diagdown \\ \diagup \end{array} = -i\lambda_{HHHH} \equiv -i\kappa_4\lambda_{HHHH}^{\text{SM}},$$

where  $\kappa_3 \equiv \lambda_{HHH}/\lambda_{HHH}^{\text{SM}}$  and  $\kappa_4 \equiv \lambda_{HHHH}/\lambda_{HHHH}^{\text{SM}}$  are the parameters that we introduced in the EChL. Remember that within the SM ( $\kappa_3 = \kappa_4 = 1$ ) these two couplings are correlated by  $\lambda_{HHH}^{\text{SM}} = \lambda_{HHHH}^{\text{SM}}$ . In contrast, in BSM scenarios, we will generally find

$\kappa_3 \neq 1$  and/or  $\kappa_4 \neq 1$  and this correlation could be lost.

This redefinition can be easily implemented in FEYNARTS-3.10, allowing us to compute the new cross sections in the same manner as we have done for the SM. The results of these calculations are shown in figures 3.5 to 3.7, in which we show the behaviour of the cross section with energy for different values of  $\kappa_3$  and  $\kappa_4$ , and figures 3.8 to 3.10, in which we compute the cross section at fixed energies to observe the variation with  $\kappa_3$  and  $\kappa_4$ , independently. Note that since double Higgs production does not involve the quartic coupling (at least at tree level), the value of  $\kappa_4$  is not relevant for the predictions.

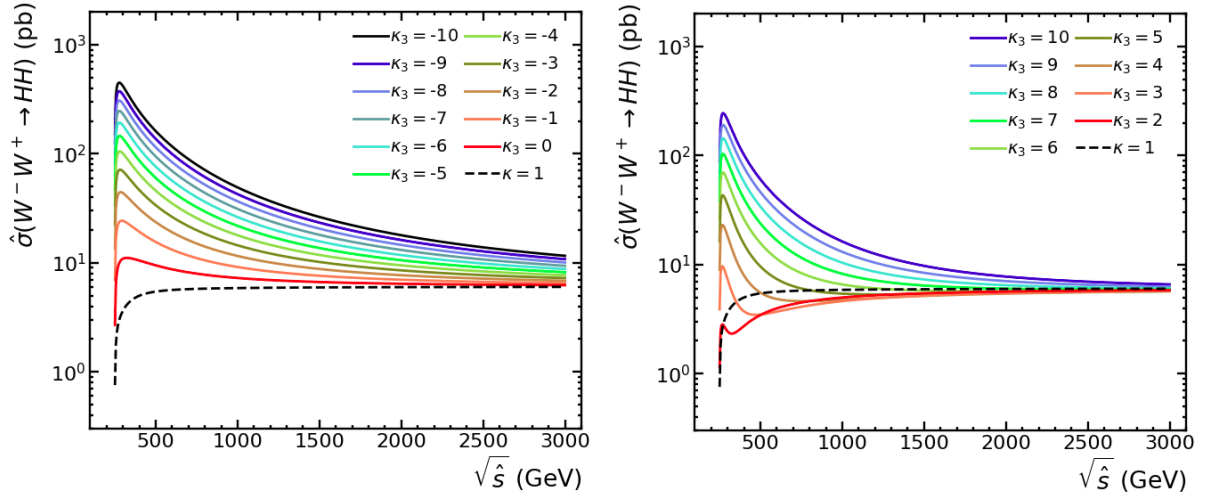


**Figure 3.5:** Total cross section of the  $W^-W^+ \rightarrow HH$  subprocess as a function of the CM energy  $\sqrt{\hat{s}}$  for different values of the parameter  $\kappa_3$ , with  $\kappa_4$  fixed to 1, compared to the SM prediction (dashed line).

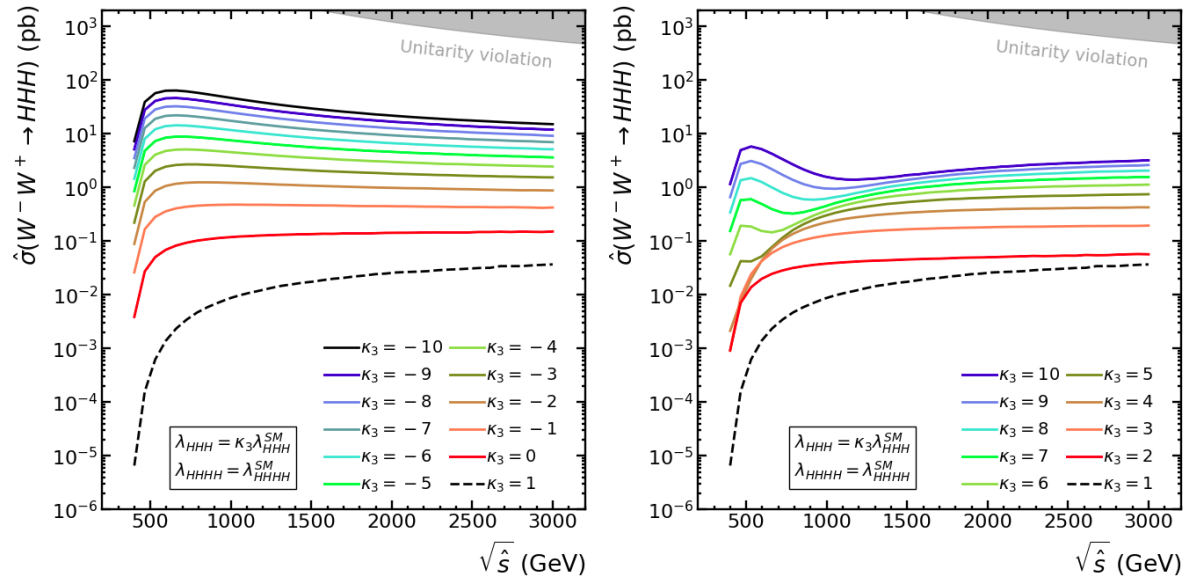


**Figure 3.6:** Total cross section of the  $W^-W^+ \rightarrow HHH$  subprocess as a function of the CM energy  $\sqrt{\hat{s}}$  for different values of the parameter  $\kappa_3$ , with  $\kappa_4$  fixed to 1, compared to the SM prediction (dashed line).

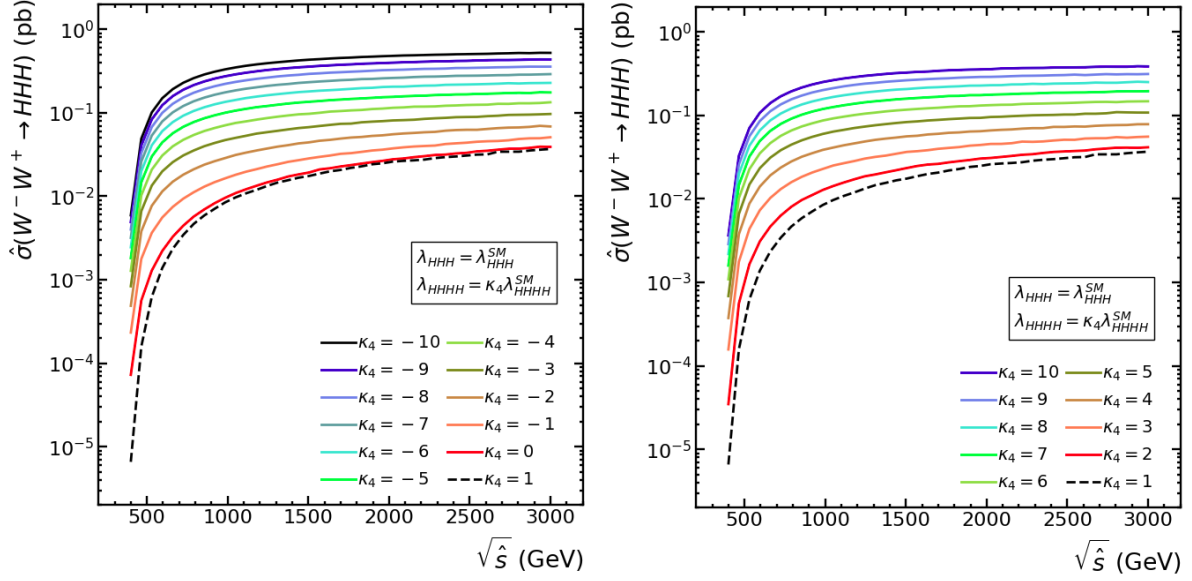


**Figure 3.7:** Total cross section of the  $W^-W^+ \rightarrow HHH$  subprocess as a function of the CM energy  $\sqrt{\hat{s}}$  for different values of the parameter  $\kappa_4$ , with  $\kappa_3$  fixed to 1, compared to the SM prediction (dashed line).

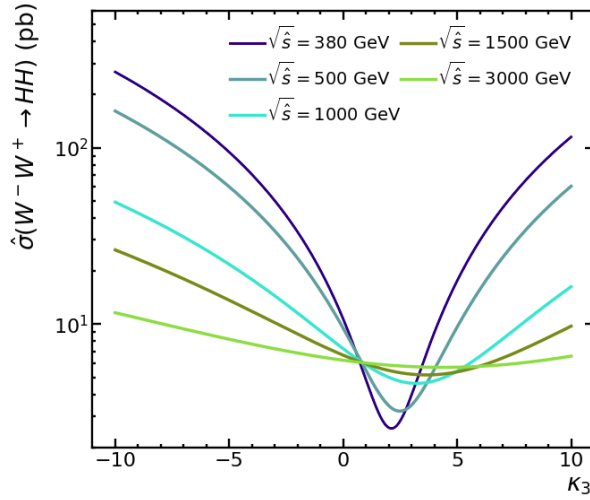


**Figure 3.8:** Total cross section of the  $W^-W^+ \rightarrow HH$  subprocess as a function of  $\kappa_3$  (with  $\kappa_4$  fixed to 1) for different values of the CM energy  $\sqrt{\hat{s}}$ .

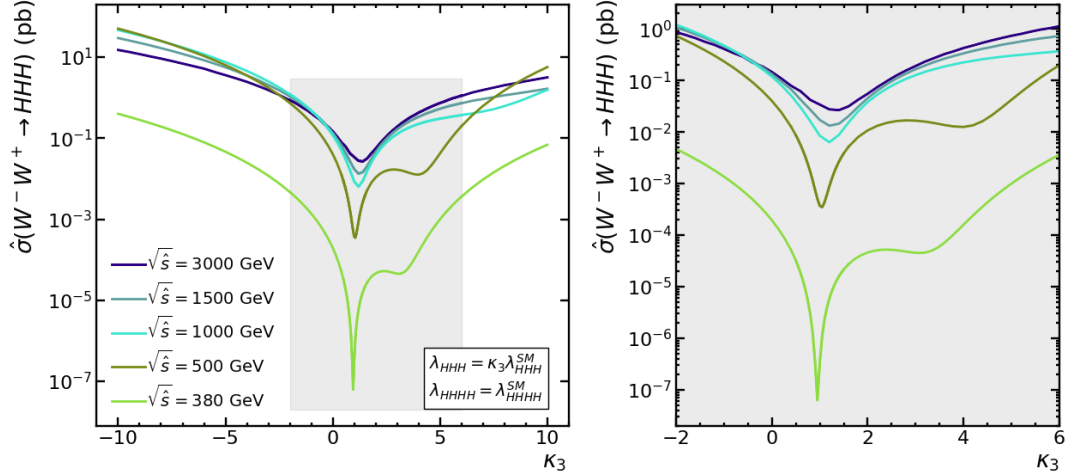


**Figure 3.9:** Total cross section of the  $W^-W^+ \rightarrow HHH$  subprocess as a function of  $\kappa_3$  (with  $\kappa_4$  fixed to 1) for different values of the CM energy  $\sqrt{\hat{s}}$ .

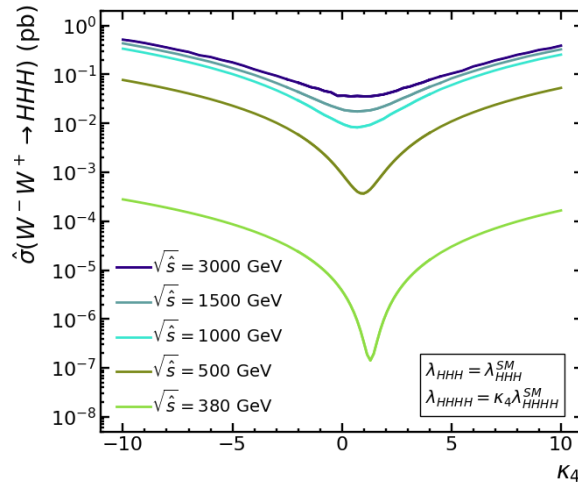


**Figure 3.10:** Total cross section of the  $W^-W^+ \rightarrow HHH$  subprocess as a function of  $\kappa_4$  (with  $\kappa_3$  fixed to 1) for different values of the CM energy  $\sqrt{\hat{s}}$ .

We can extract some first conclusions by looking at these plots. Starting from figure 3.5, we observe that modifying  $\kappa_3$  in the interval  $[-10,10]$  with  $\kappa_4$  fixed to 1 leads to a notable enhancement in the total cross section with respect to the SM prediction, here represented by the dashed line ( $\kappa_3 = 1$ ). The maximum deviation occurs slightly above the threshold energy  $2m_H$ , and it is larger for negative values of  $\kappa_3$ . In the most extreme case,  $\kappa_3 = -10$ , the BSM prediction can deviate up to two orders of magnitude with respect to the SM value.

Figure 3.6 shows that the consequences of modifying  $\kappa_3$  at  $\kappa_4$  fixed to 1 are similar in the case of triple Higgs production, but now the maximum is produced slightly above the new threshold energy,  $3m_H$ . The deviations with respect to the SM are larger again for negative values of  $\kappa_3$ , and can reach a difference of five orders of magnitude with respect to the SM. Varying the value of  $\kappa_4$  with  $\kappa_3$  fixed to 1 (figure 3.7) does not modify the

shape of the cross section significantly, but can increase its value by one or even two orders of magnitude in the most extreme cases. The dependence on the sign of  $\kappa_4$ , in contrast with the previous plots, is very mild.

Coming back to  $W^-W^+ \rightarrow HH$ , figure 3.8 shows the variation of the cross section with  $\kappa_3$  at a fixed CM energy. Here we see that there is a minimum in the region  $\kappa_3 \in [2, 5]$  that moves to the right in this interval, being closer to 2 at  $\sqrt{\hat{s}} = 380$  GeV and closer to 5 at  $\sqrt{\hat{s}} = 3000$  GeV. Deviations from the SM can go up to two orders of magnitude in the most extreme case, that is, for  $\kappa_3 = -10$  at the lowest energy. The sensitivity to variations of the  $\kappa_3$  parameter decreases with increasing energy; note that outside the region of the minimum, the cross sections are inverted, being higher at lower energies. This is the peak that we see in figure 3.5 near the threshold for BSM values of the self-couplings that does not appear in the SM case.

When reproducing this same plot for  $W^-W^+ \rightarrow HHH$  as a function of  $\kappa_3$  (figure 3.9) we find a very different picture. First of all, the peak is displaced in energy, so the maximum is reached around  $\sqrt{\hat{s}} = 500$  GeV. This is why the cross section at  $\sqrt{\hat{s}} = 380$  GeV is always small, in comparison to what we have seen in the  $HH$  case. Second, the shape of the curve, specially at low energies, exhibits two minima instead of one. One of them is near the SM value  $\kappa_3 = 1$ , and the other one appears at positive  $\kappa_3$  and is displaced to higher values of this parameter as energy grows. The maximum deviations with respect to the SM are large in any case, varying from two orders of magnitude at  $\sqrt{\hat{s}} = 3000$  GeV to even seven orders of magnitude at  $\sqrt{\hat{s}} = 380$  GeV. This cross section is significantly more sensitive to variations in the  $\kappa_3$  parameter than  $\sigma(W^-W^+ \rightarrow HH)$ , mainly at low energies, having the disadvantage that it is much lower in general.

Finally, figure 3.10 shows the dependence with the  $\kappa_4$  parameter, which only exhibits one minimum per curve. In this case, the maximum deviations from the SM vary from one order of magnitude at  $\sqrt{\hat{s}} = 3000$  GeV to three orders of magnitude at  $\sqrt{\hat{s}} = 380$  GeV.

Since triple Higgs production depends on both the  $\kappa_3$  and  $\kappa_4$  parameters, it is also interesting to check what happens if we vary the two of them at the same time. In figure 3.11 we represent the  $W^-W^+ \rightarrow HHH$  cross section at three fixed energies ( $\sqrt{\hat{s}} = 500, 1000$  and  $3000$  GeV) in the  $(\kappa_3, \kappa_4)$  plane. The additional information that we can extract looking at these plots is that variations in the cross section are strongly dominated by deviations along the  $\kappa_3$  direction, and the higher values are reached when  $\kappa_3$  approaches  $-10$ . The dependence with  $\kappa_4$  is softer, and the maximum cross section can be reached either at negative or positive values of  $\kappa_4$ ; for example, in the negative  $\kappa_3$  region (approximately) the cross section tends to be higher around  $\kappa_4 = 10$ , while in the positive  $\kappa_3$  region the trend can be the same or the opposite depending on the energy. Note that at high energies the combined effect of modifying both parameters at the same

time can lead to an increase of the cross section, specially if they have opposite signs. We also notice that the lowest values (darker region) are arranged in a diagonal direction which is not the  $\kappa_3 = \kappa_4$  direction, which means that modifying the Higgs self couplings without altering the ratio between them, that is,  $\lambda_{HHH}/\lambda_{HHHH} = \lambda_{HHH}^{\text{SM}}/\lambda_{HHHH}^{\text{SM}} = 1$ , can also produce an enhancement in the cross section. The size of this darker region is related to the depth of the minimum, and is smaller for lower energies. Note that the SM value is contained in this region, which is why we do not expect to measure this process if the self-couplings are close to the SM. In any case, what we are studying here is the subprocess, which can not be seen in a real experiment, so to complete our analysis, in the next section we will calculate the full process to understand how sensitive we are to deviations in these parameters.

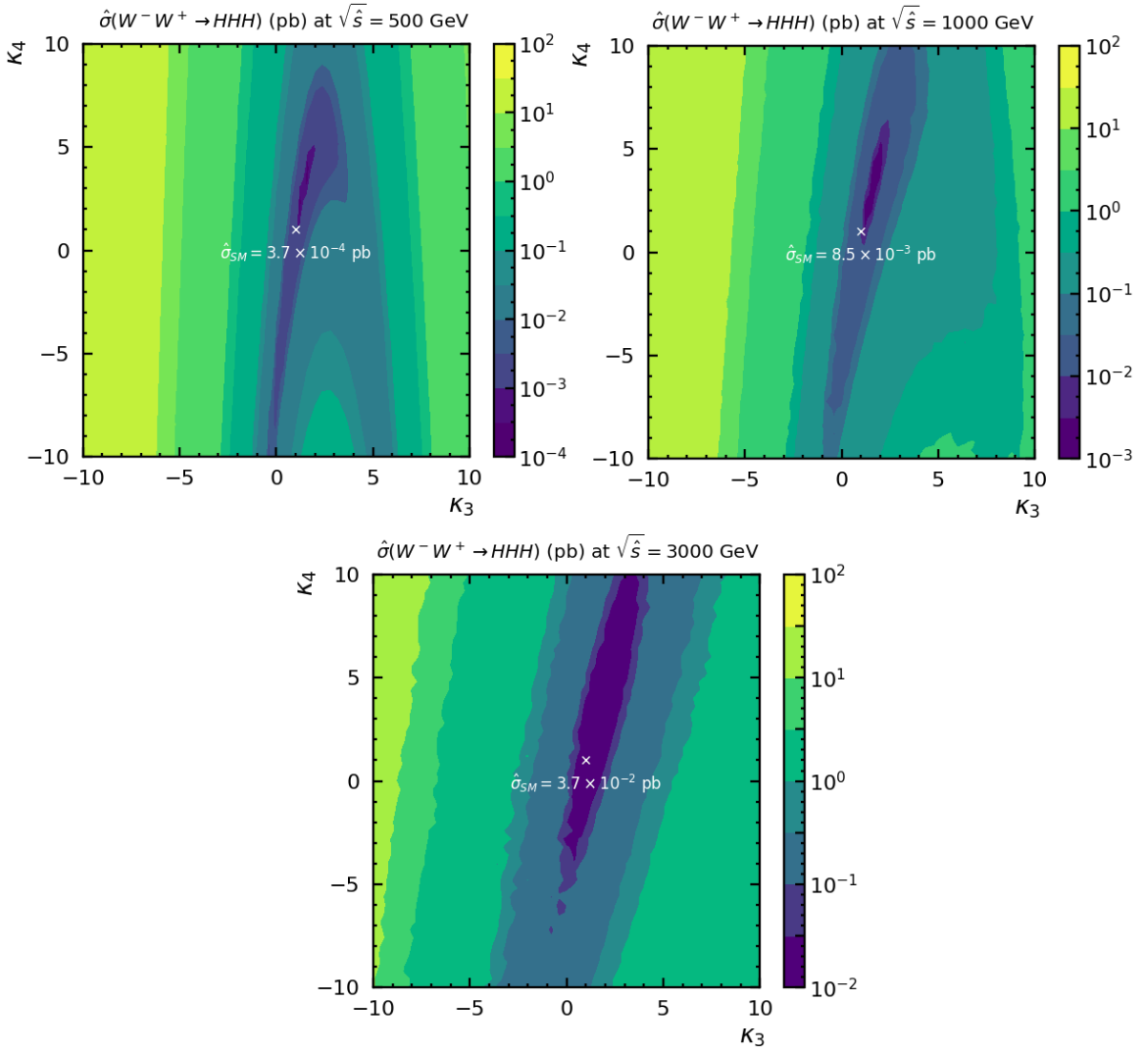


**Figure 3.11:** Contour levels for the total cross section of the  $W^-W^+ \rightarrow HHH$  subprocess represented in the  $(\kappa_3, \kappa_4)$  plane for different values of the CM energy  $\sqrt{\hat{s}}$ .

Regarding unitarity, we can confirm that the  $W^-W^+ \rightarrow HHH$  subprocess does not

violate unitarity for any value of the BSM self-couplings that we have studied so far, in the range of energies that we are interested in. In the worst-case scenario ( $\sqrt{\hat{s}} = 3000$  GeV), preservation of unitarity requires that:

$$\hat{\sigma}(W^-W^+ \rightarrow HHH) \lesssim 540 \text{ pb}, \quad (3.7)$$

which is not reached even in the most extreme cases in figure 3.11. This result could be expected from the beginning, taking into account that the Higgs boson self-couplings are not responsible for very strong cancellations in the SM amplitudes, as it is the case of the vector boson couplings. In fact, the SM Higgs boson couples to vector bosons in such a way that it perfectly cancels the divergent contributions coming from longitudinal vector boson scattering, which grow as the energy squared and violate unitarity in the TeV scale. An example of the consequences of modifying these parameters can be found in [24].

## 4 Testing the BSM Higgs self-couplings via triple Higgs production at $e^-e^+$ colliders

Characterizing the  $W^-W^+ \rightarrow HHH$  subprocess is an interesting way of studying deviations from the SM and putting limits on the value of the Higgs self-couplings from BSM physics. However, the information obtained from this study is not complete. To be able to make phenomenological predictions it is necessary to remember that in a real collider we do not have  $W$  bosons in the initial state, but only protons or electrons. As we already mentioned before, in this work we will focus on the case of an  $e^-e^+$  linear collider, such as the ILC or CLIC, for several reasons. To begin with, due to the fundamental character of the colliding particles (in contrast with the hadronic nature of protons) the initial state is well defined; in the case of proton-proton collisions the energy of the partons that collide is a priori unknown and a significant amount of the initial energy of the protons is wasted due to the effect of the Parton Distribution Functions (PDFs) of the proton. In addition, QCD backgrounds in  $e^-e^+$  colliders are less dominant, allowing us to study Higgs decay channels such as  $H \rightarrow b\bar{b}$  with less difficulties. Moreover, although the study of multiple Higgs production in very high energy proton-proton colliders has been considered in the literature, it has not been practically explored in linear colliders due to its low SM cross section. Therefore, the conclusions about the Higgs self-couplings obtained from this work perfectly complement what has already been studied by other authors. In particular, the joint study of the two BSM couplings,  $\lambda_{HHH}$  and  $\lambda_{HHHH}$  in  $e^-e^+$  colliders presented here is, to our knowledge, the first one in the literature.

## 4.1 WWS in $e^-e^+$ colliders

Before starting our analysis, it is interesting to study the behaviour of the most important multiple Higgs production mechanisms in  $e^-e^+$  colliders at different energies. There are several possible production mechanisms that can yield multiple Higgs bosons in the final state, but due to the low statistics it is convenient to use those that exhibit a higher cross section. This is the reason why in this work we will focus our attention in multiple Higgs production with neutrinos in the final state,  $e^-e^+ \rightarrow HH(H)\nu\bar{\nu}$ . In order to better understand this process we have generated a set of plots using MADGRAPH 5, which describe the behaviour of the  $e^-e^+ \rightarrow HH(H)\nu\bar{\nu}$  process as well as its different contributions.

Figure 4.1 shows that the dominant contribution to  $\sigma(e^-e^+ \rightarrow HH(H)\nu\bar{\nu})$  at low energies comes from associated production of two (three)  $H$ 's with a  $Z$  boson, also denoted as  $ZHH(H)$ . The cross section for this particular production mechanism can be computed as the cross section of the process  $e^-e^+ \rightarrow ZHH(H)$  times the branching ratio  $\text{BR}(Z \rightarrow \text{invisible}) = 20\%$ . The corresponding curve shows how it becomes subdominant as the energy increases, meaning that  $ZHH(H)$  is not the main production mechanism for  $HH(H)\nu\bar{\nu}$  in the TeV scale.

If we now move to figure 4.2, we see that the enhancement in  $\sigma(e^-e^+ \rightarrow HH(H)\nu\bar{\nu})$  at high energies actually comes from  $\sigma(e^-e^+ \rightarrow HH(H)\nu_e\bar{\nu}_e)$ , that is, processes with electron neutrinos in the final state. The contribution from  $\sigma(e^-e^+ \rightarrow HH(H)\nu_\mu\bar{\nu}_\mu)$  is also represented, and it is seen that it decreases as we go to higher energies<sup>4</sup>.

In figure 4.3 we can see that the origin of the enhancement in  $\sigma(e^-e^+ \rightarrow HH(H)\nu\bar{\nu})$ , and in particular in  $\sigma(e^-e^+ \rightarrow HH(H)\nu_e\bar{\nu}_e)$ , are the  $WW$  scattering (WWS) diagrams because the probability for an electron to radiate a  $W$  boson increases when this electron is more energetic, together with the behaviour of the WWS subprocess with energy, already seen in the previous section. Note that diagrams contributing to  $\sigma(e^-e^+ \rightarrow HH(H)\nu_e\bar{\nu}_e)$  at the lowest order can be of two types, WWS or  $ZHH(H)$ , so if we compute  $\sigma(e^-e^+ \rightarrow HH(H)\nu_\mu\bar{\nu}_\mu)$  the WWS diagrams vanish. The surviving diagrams are what we define as the  $ZHH(H)$  contribution to  $\sigma(e^-e^+ \rightarrow HH(H)\nu_e\bar{\nu}_e)$ , since  $\text{BR}(Z \rightarrow \nu_e\bar{\nu}_e) = \text{BR}(Z \rightarrow \nu_\mu\bar{\nu}_\mu)$ , where BR refers to the branching ratio of the  $Z$  boson. Then, the contribution to  $\sigma(e^-e^+ \rightarrow HH(H)\nu_e\bar{\nu}_e)$  coming from WWS can be isolated using the following ‘‘theoretical observable’’:

$$\sigma_{\text{WWS}} = \sigma(e^-e^+ \rightarrow HH(H)\nu_e\bar{\nu}_e) - \sigma(e^-e^+ \rightarrow HH(H)\nu_\mu\bar{\nu}_\mu), \quad (4.1)$$

<sup>4</sup>The cross section for the process  $e^-e^+ \rightarrow HH(H)\nu_\tau\bar{\nu}_\tau$  is in principle the same as  $\sigma(e^-e^+ \rightarrow HH(H)\nu_\mu\bar{\nu}_\mu)$ , but it is not represented for simplicity.

which is what we plot in figure 4.3. It is also important to notice that  $ZZ$  scattering ( $ZZS$ ) contributes to the final state  $HH(H)e^-e^+$ , which has a much lower production cross section (the probability of producing two or three Higgs bosons via  $ZZS$  is approximately ten times lower), and therefore will be neglected in this work.

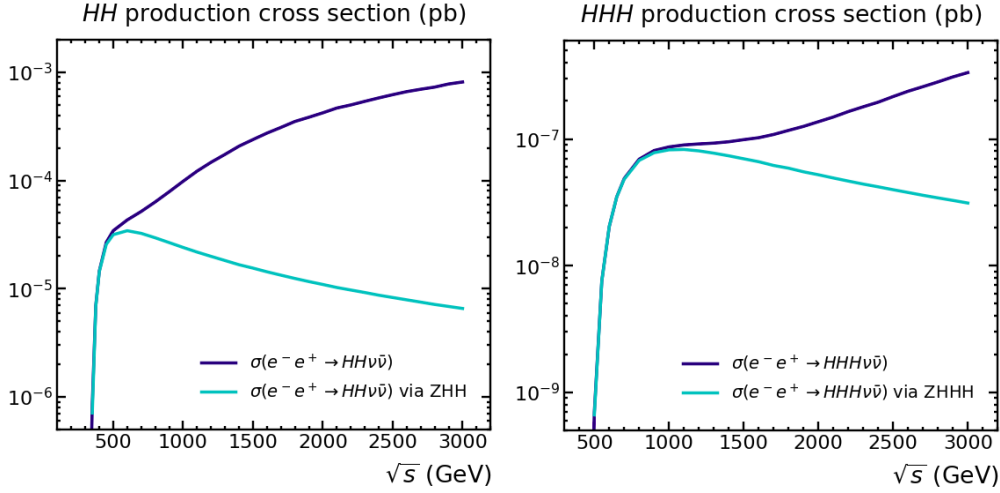


**Figure 4.1:** Predictions for  $\sigma(e^-e^+ \rightarrow HH\nu\bar{\nu})$  (left) and  $\sigma(e^-e^+ \rightarrow HHH\nu\bar{\nu})$  (right) in the SM as a function of the CM energy  $\sqrt{s}$ . The corresponding cross sections coming from just the  $Z$  mediated subprocesses,  $\sigma(e^-e^+ \rightarrow ZHH \rightarrow HH\nu\bar{\nu})$  and  $\sigma(e^-e^+ \rightarrow ZHHH \rightarrow HHH\nu\bar{\nu})$  are also shown for comparison.

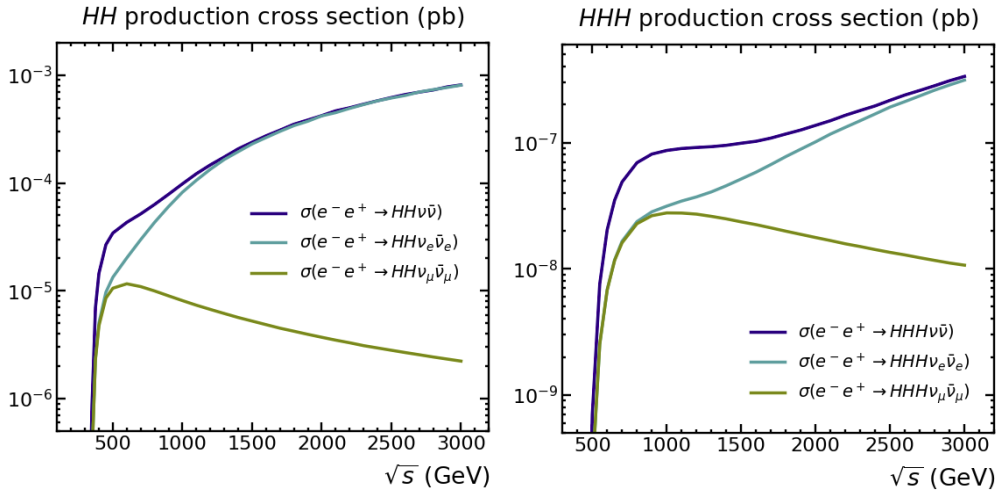


**Figure 4.2:** Predictions for  $\sigma(e^-e^+ \rightarrow HH\nu_e\bar{\nu}_e)$  and  $\sigma(e^-e^+ \rightarrow HH\nu_\mu\bar{\nu}_\mu)$  (left) and  $\sigma(e^-e^+ \rightarrow HHH\nu_e\bar{\nu}_e)$  and  $\sigma(e^-e^+ \rightarrow HHH\nu_\mu\bar{\nu}_\mu)$  (right) in the SM as a function of the CM energy  $\sqrt{s}$ . The cross sections for  $e^-e^+ \rightarrow HH\nu\bar{\nu}$  and  $e^-e^+ \rightarrow HHH\nu\bar{\nu}$  from previous figure are also shown for comparison.

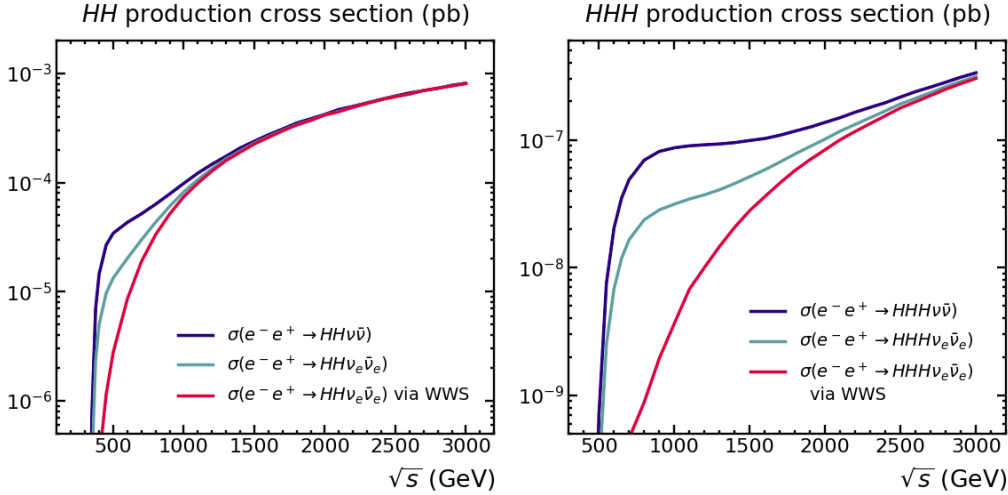


**Figure 4.3:** Double (left) and triple (right) Higgs production cross section in  $e^-e^+$  collisions with neutrinos in the final state and the corresponding contributions coming from  $HH(H)\nu_e\bar{\nu}_e$  and WWS.

Although the previous figures show separate contributions to  $\sigma(e^-e^+ \rightarrow HH(H)\nu\bar{\nu})$ , one must realize that in the experiment it is only possible to measure  $\sigma(e^-e^+ \rightarrow HH(H)\nu\bar{\nu})$ , since there is no way to distinguish among the different neutrino flavours, and even if we could, the result of separating the WWS diagrams from  $\sigma(e^-e^+ \rightarrow HH(H)\nu_e\bar{\nu}_e)$  would not be gauge invariant. The reason why we do this subtraction is to show in a gauge invariant way that WWS is the largest contribution at high energies and, as a consequence, the predictions for  $\sigma(e^-e^+ \rightarrow HH(H)\nu\bar{\nu})$  will approximately follow its behaviour, and more generally, the behaviour of  $\sigma(e^-e^+ \rightarrow HH(H)\nu_e\bar{\nu}_e)$ .

Comparing triple with double Higgs production in figures 4.1, 4.2 and 4.3, we find that they are roughly similar in shape, being the WWS enhancement in triple Higgs production displaced to higher energies, since one extra particle is produced. This causes that  $ZHHH$  is more relevant compared to  $HHH\nu\bar{\nu}$  than  $ZHH$  compared to  $HH\nu\bar{\nu}$ , specially at energies below 2000 GeV. It is also important to note that the SM cross sections for triple Higgs production in the TeV energy scale are typically three orders of magnitude below than those of double Higgs production, which is why it is not expected to measure SM-like  $HHH$  production in future linear colliders. For this reason, we will focus our attention in BSM scenarios.

## 4.2 The effective $W$ approximation

Due to the nature of the WWS process, it can be useful in some cases to factorize the calculation of the cross section into the emission of the  $W$  bosons and their subsequent scattering. This method is called the effective  $W$  approximation (EWA) [46], which is a generalization of the effective photon approximation. It consists on treating the vector

bosons that are radiated from the electrons as if they were partons in a proton, with their corresponding distribution functions. This approximation simplifies the calculation of the cross section significantly, and offers a more analytical and intuitive approach. In this section we will briefly introduce the EWA, review its validity in double Higgs production and see if it can be used in triple Higgs production.

According to the EWA,  $W$  (or  $Z$ ) bosons radiated from a fermion can be treated as partons inside a proton. This allows to define distribution functions for these bosons equivalent to the PDFs of quarks and gluons inside the proton (figure 4.4). The corresponding analytical expressions for these distributions are [46]:

$$\begin{aligned}
f_T(x) &= \left( \frac{C_V^2 + C_A^2}{8\pi^2 x} \right) \left[ \frac{-x^2}{1 + m_W^2/[4E^2(1-x)]} + \frac{2x^2(1-x)}{m_W^2/E^2 - x^2} \right. \\
&\quad \left. + \left\{ x^2 + \frac{x^4(1-x)}{(m_W^2/E^2 - x^2)^2} \left( 2 + \frac{m_W^2}{E^2(1-x)} \right) - \frac{x^2}{(m_W^2/E^2 - x^2)^2} \frac{m_W^4}{2E^4} \right\} \right. \\
&\quad \left. \times \log \left( 1 + \frac{4E^2(1-x)}{m_W^2} \right) + x^4 \left( \frac{2-x}{m_W^2/E^2 - x^2} \right)^2 \log \left( \frac{x}{2-x} \right) \right] \eta, \\
f_L(x) &= \left( \frac{C_V^2 + C_A^2}{\pi^2} \right) \left( \frac{1-x}{x} \right) \left( \frac{\eta}{(1+\eta)^2} \right) \left\{ \frac{1-x - m_W^2/(8E^2)}{1-x + m_W^2/(4E^2)} \right. \\
&\quad \left. - \frac{m_W^2}{4E^2} \frac{1 + 2(1-x)^2}{(1-x) + m_W^2/(4E^2)} \frac{1}{m_W^2/E^2 - x^2} - \frac{m_W^2}{4E^2} \left( \frac{x^2}{2(1-x)(x^2 - m_W^2/E^2)^2} \right) \right. \\
&\quad \left. \times \left[ (2-x)^2 \log \left( \frac{x}{2-x} \right) - \left( \left[ x - \frac{m_W^2}{E^2 x} \right]^2 - [2(1-x) + x^2] \right) \log \left( 1 + \frac{4E^2(1-x)}{m_W^2} \right) \right] \right. \\
&\quad \left. - \frac{m_W^2}{8E^2} \frac{x}{\sqrt{x^2 - m_W^2/E^2}} \left( \frac{2}{x^2 - m_W^2/E^2} + \frac{1}{1-x} \right) \left( \log \frac{2-x - \sqrt{x^2 - m_W^2/E^2}}{2-x + \sqrt{x^2 - m_W^2/E^2}} \right. \right. \\
&\quad \left. \left. - \log \frac{x - \sqrt{x^2 - m_W^2/E^2}}{x + \sqrt{x^2 - m_W^2/E^2}} \right) \right], \\
\eta &= \left( 1 - \frac{m_W^2}{x^2 E^2} \right)^{1/2}, \tag{4.2}
\end{aligned}$$

where L refers to a longitudinally polarized  $W$  boson and T to a transversely polarized  $W$  boson,  $C_V = -C_A = g/(2\sqrt{2})$  and  $E$  is the energy of the initial fermions, which can also be written as  $\sqrt{s}/2$  (note that the expressions vary if we have  $Z$  bosons instead). The bosons are assumed to be radiated collinearly and then scatter on-shell, so the computation of the total cross section can be factored as:

$$\sigma(s) = \int dx_1 \int dx_2 \sum_{i,j} f_i(x_1) f_j(x_2) \hat{\sigma}_{ij}(\hat{s}). \quad (4.3)$$

Here,  $\sigma(s) = \sigma(e^-e^+ \rightarrow HH(H)\nu_e\bar{\nu}_e)$  is the total cross section of the process of interest at a CM energy of  $\sqrt{s}$  and  $\hat{\sigma}_{ij}(\hat{s}) = \hat{\sigma}(W_iW_j \rightarrow HH(H))$  is the cross section of the subprocess at a CM energy of  $\sqrt{\hat{s}}$ . Note that even if the two  $W$  bosons do not have the same energy and opposite momentum (CM frame), the condition that they are collinear to the initial fermions allows us to use the same cross section that we computed in the previous chapter, due to the invariance of the cross section under boosts along the  $z$  direction.  $x_1$  and  $x_2$  are the momentum fractions carried by each  $W$  boson and define the CM energy of the subprocess as  $\sqrt{\hat{s}} = \sqrt{x_1x_2s}$ . The subindices  $i, j$  refer to the polarization of the  $W$  bosons (L or T). They are necessary because the probability of radiating an  $W$  boson depends on whether it is longitudinally or transversely polarized, and consequently, each polarized cross section is convoluted with the corresponding combination of distribution functions  $f_i(x)$ . Note that this formula assumes that WWS is the dominant contribution to  $\sigma(e^-e^+ \rightarrow HH(H)\nu_e\bar{\nu}_e)$ , which makes it valid only at high energies. To compute this cross section we write  $\hat{\sigma}_{ij}(\hat{s})$  in terms of the polarized amplitudes  $\mathcal{M}_{ij}$ , which we generate using FEYNARTS-3.10 and FORMCALC-9.6, and then perform the integration using VEGAS and a private Python code:

$$\sigma(s) = \int dx_1 \int dx_2 \frac{1}{3!} \frac{1}{2\sqrt{\hat{s}^2 - 4\hat{s}m_W^2}} \frac{1}{32(2\pi)^4\hat{s}} \int dm_{34}^2 \int dm_{45}^2 \int d\cos\theta_3 \int d\phi_{35} \sum_{i,j} f_i(x_1) f_j(x_2) |\overline{\mathcal{M}}_{ij}|^2. \quad (4.4)$$

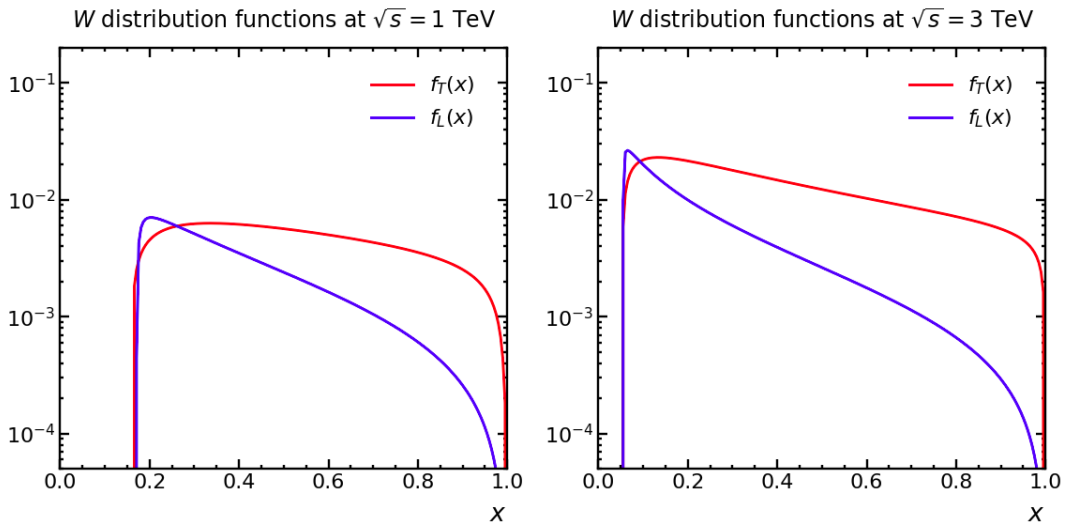


**Figure 4.4:** Probability for an electron of energy 0.5 TeV (left) and 1.5 TeV (right) to radiate a  $W$  boson (longitudinal/L or transverse/T) with momentum fraction  $x$ , taken from equation 4.2. Except for very low  $x$ , in both cases the probability is higher for a transverse  $W$ . The comparison shows how the probability increases with the electron energy.

To see if the EWA is suitable for describing triple Higgs production, we first calculate the total cross section of the process  $e^-e^+ \rightarrow HHH\nu_e\bar{\nu}_e$  at different values of the CM energy (figure 4.5), as well as the corresponding polarized cross sections (figure 4.6). The same plots have also been produced in the case of double Higgs production for comparison.

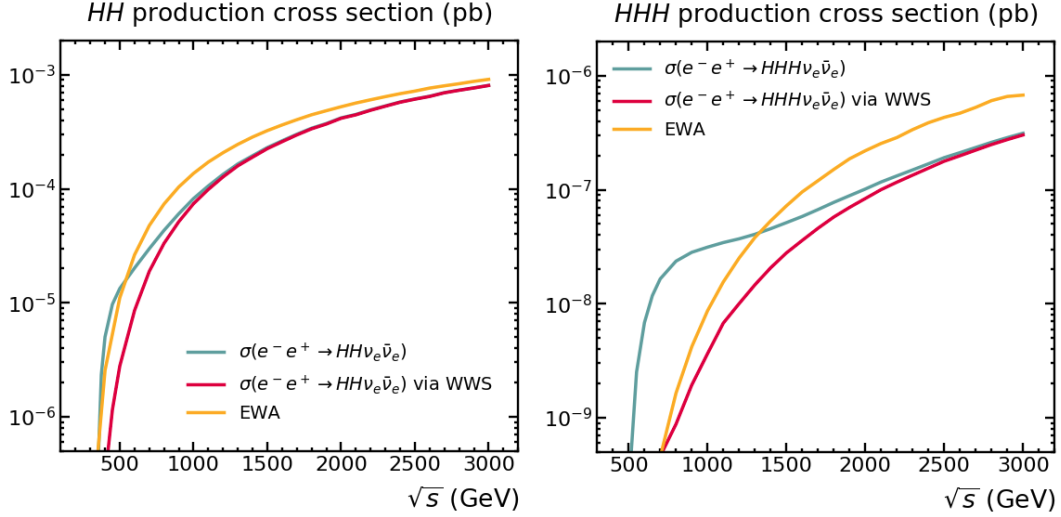


**Figure 4.5:** EWA compared to  $HH(H)\nu_e\bar{\nu}_e$  and its WWS contribution in double Higgs (left) and triple Higgs (right) production.

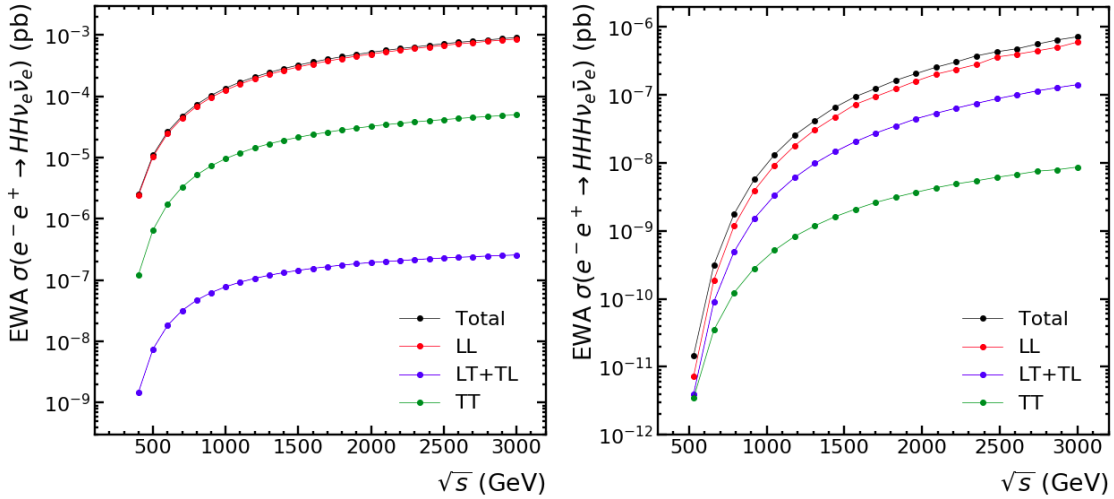


**Figure 4.6:** Polarized contributions to  $\sigma(e^-e^+ \rightarrow HH\nu_e\bar{\nu}_e)$  (left) and  $\sigma(e^-e^+ \rightarrow HHH\nu_e\bar{\nu}_e)$  (right) using the EWA.

Starting from figure 4.5, the EWA is compared with the  $e^-e^+ \rightarrow HH(H)\nu_e\bar{\nu}_e$  cross section obtained from MADGRAPH 5 and its WWS contribution, calculated using equation 4.1. What we see is that at high energies the EWA predicts the  $HH$  production cross section with good accuracy, while it differs about a factor of two for the  $HHH$  case. The energies that we are considering in this work seem to be too low for the EWA to be a

good approximation of triple Higgs production.

Moving now to figure 4.6, we observe that the dominant contribution comes from longitudinally polarized  $W$  bosons in both cases. The main differences are that the gap between LL and TT is larger for  $HHH$  production and that the relative size of the TT and LT+TL polarizations is interchanged with respect to the  $HH$  case. For  $HHH$ , the TT contribution is subdominant by up to two orders of magnitude with respect to the LL one. This difference is smaller in the  $HH$  case. Note how all contributions grow with energy in contrast with what we saw for the corresponding subprocesses in the previous section due to the folding with the  $W$  distribution functions.

Another condition for the EWA to be a useful approximation is that it can reproduce the differential cross section distributions. As an example, figure 4.7 shows the differential cross section with respect to the invariant mass of the final state Higgs bosons,  $M_{HH}$  and  $M_{HHH}$  respectively, which is equivalent to  $\sqrt{\hat{s}}$  due to 4-momentum conservation. The results are again positive for double Higgs production, but do not adjust so well in the case of having three Higgs bosons.

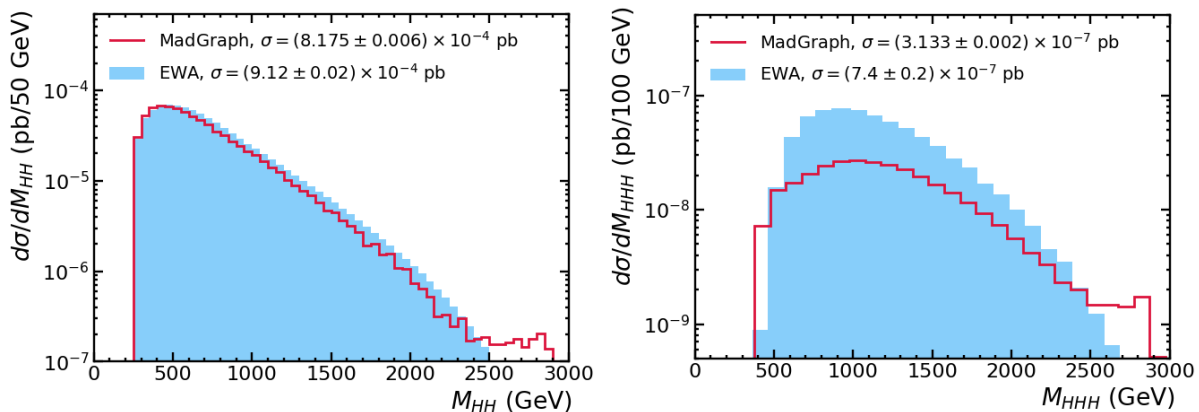


**Figure 4.7:** Differential cross section at  $\sqrt{s} = 3000$  GeV with respect to the invariant mass of the Higgs bosons for two (left) and three (right)  $H$ 's.

From this brief analysis we conclude that the EWA is an interesting alternative to compute our results in the double Higgs case, but it is not accurate enough to study triple Higgs production in the range of energies available at the  $e^-e^+$  colliders under consideration. From now on, we will not use the EWA anymore, and our results on total and differential cross sections will be extracted from the full Monte Carlo simulation (MADGRAPH 5).

### 4.3 SM prediction and BSM deviations from anomalous self-couplings

We will perform our analysis in this section using the same strategy as we did in section 3, this time for the whole process  $e^-e^+ \rightarrow HH(H)\nu_e\bar{\nu}_e$ . The behaviour of the cross section

with energy at different values of  $\kappa_3$  and  $\kappa_4$  is shown in figures 4.8 to 4.10. In figures 4.11 to 4.13, the dependence on  $\kappa_3$  and  $\kappa_4$  at fixed energies is represented.

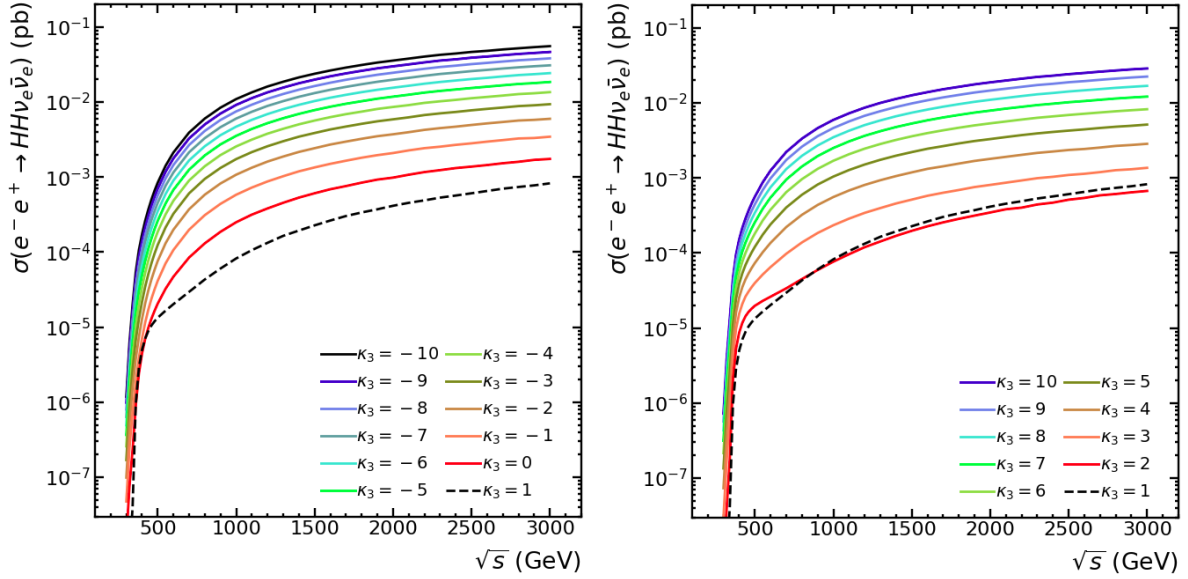


**Figure 4.8:** Total cross section of  $e^-e^+ \rightarrow HH\nu_e\bar{\nu}_e$  as a function of the CM energy  $\sqrt{s}$  for different values of the parameter  $\kappa_3$ , with  $\kappa_4$  fixed to 1, compared to the SM prediction (dashed line).

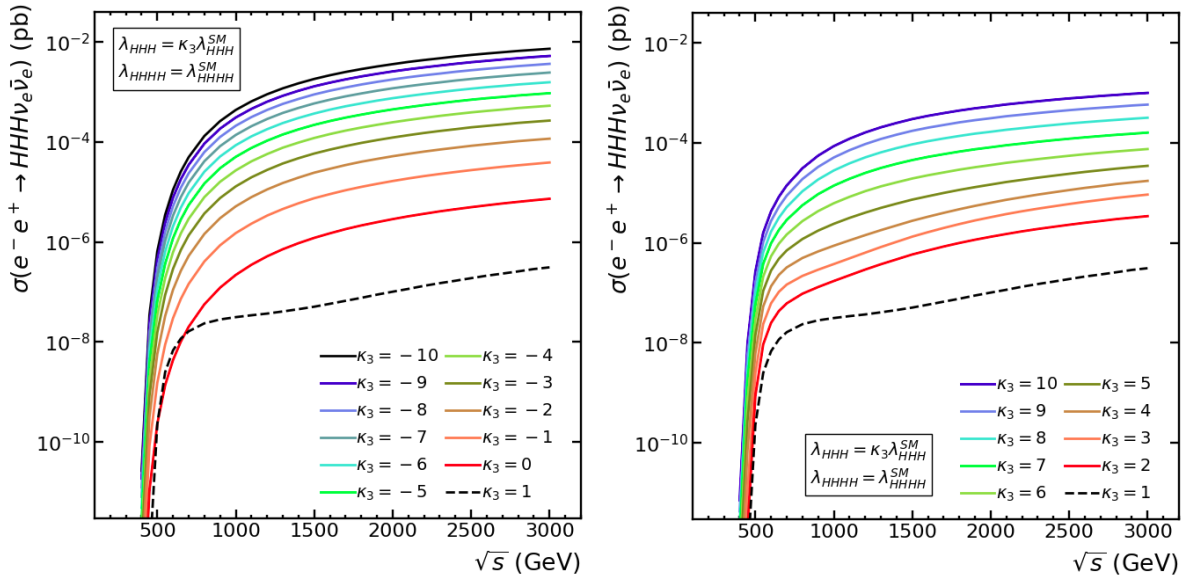


**Figure 4.9:** Total cross section of  $e^-e^+ \rightarrow HHH\nu_e\bar{\nu}_e$  as a function of the CM energy  $\sqrt{s}$  for different values of the parameter  $\kappa_3$ , with  $\kappa_4$  fixed to 1, compared to the SM prediction (dashed line).

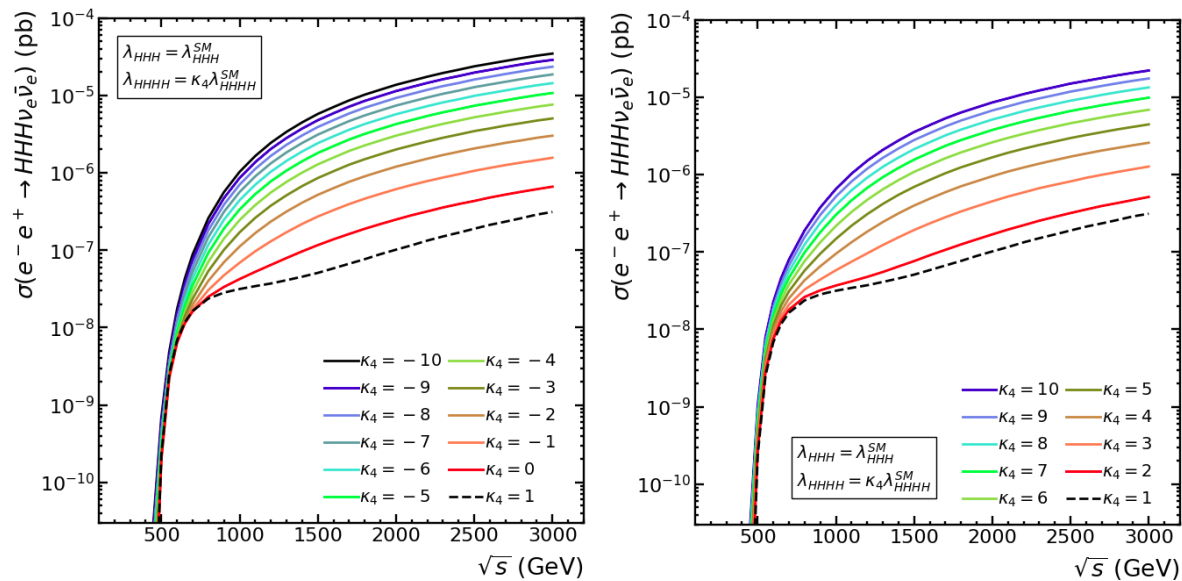


**Figure 4.10:** Total cross section of  $e^-e^+ \rightarrow HHH\nu_e\bar{\nu}_e$  as a function of the CM energy  $\sqrt{s}$  for different values of the parameter  $\kappa_4$ , with  $\kappa_3$  fixed to 1, compared to the SM prediction (dashed line).

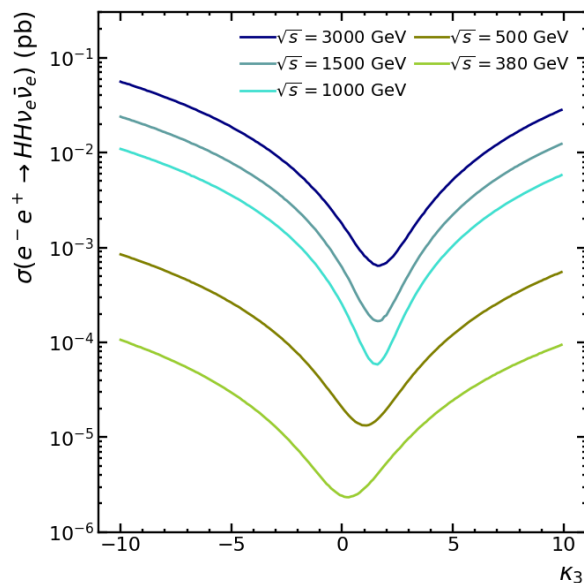


**Figure 4.11:** Total cross section of  $e^-e^+ \rightarrow HH\nu_e\bar{\nu}_e$  as a function of  $\kappa_3$  (with  $\kappa_4$  fixed to 1) for different values of the CM energy  $\sqrt{s}$ .

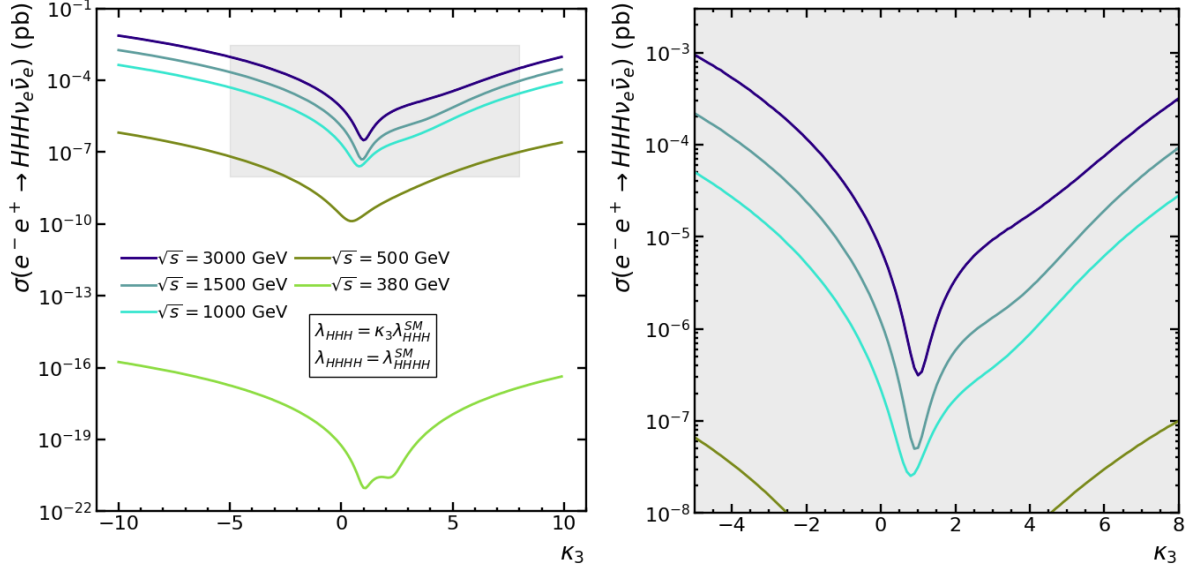


**Figure 4.12:** Total cross section of  $e^-e^+ \rightarrow HHH\nu_e\bar{\nu}_e$  as a function of  $\kappa_3$  (with  $\kappa_4$  fixed to 1) for different values of the CM energy  $\sqrt{s}$ .

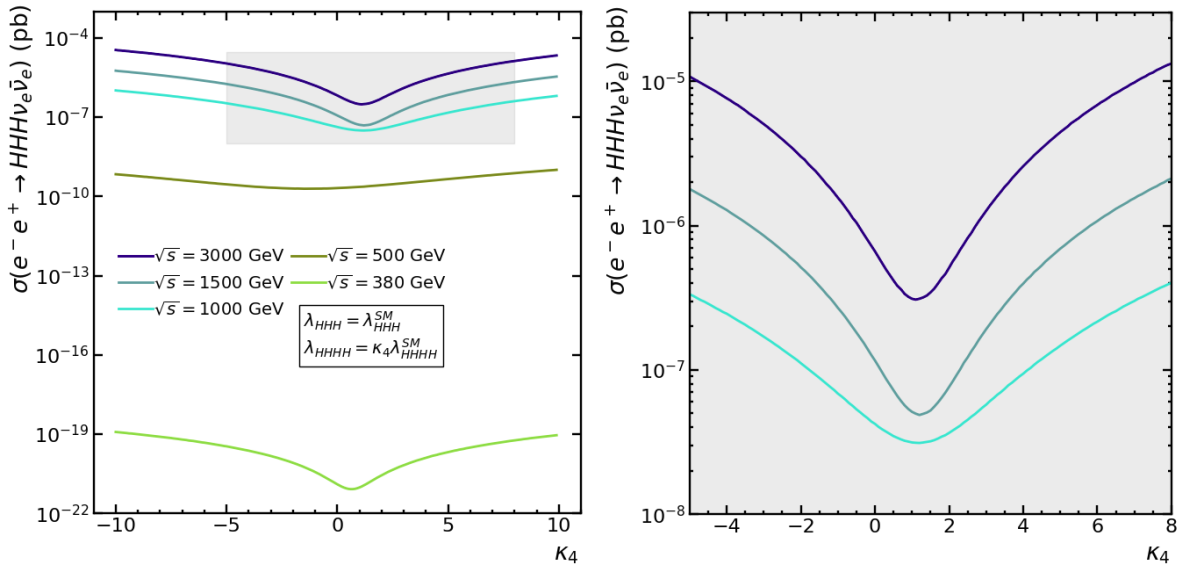


**Figure 4.13:** Total cross section of  $e^-e^+ \rightarrow HHH\nu_e\bar{\nu}_e$  as a function of  $\kappa_4$  (with  $\kappa_3$  fixed to 1) for different values of the CM energy  $\sqrt{s}$ .

Let's begin by looking at  $HH$  production in figure 4.8. In these plots we can see how, in general, deviating from  $\kappa_3 = 1$  causes an enhancement of the cross section that is approximately constant with energy. The strongest deviation occurs when  $\kappa_3 = -10$ , and it differs from the SM prediction by two orders of magnitude. Another thing that can be seen in  $HH$  production and will be more significant in  $HHH$  is that the bump near the threshold corresponding to associated  $Z$  production disappears when we deviate from the SM.

By comparing to  $HHH$  in figure 4.9, we observe something that we had already noticed in previous section: triple Higgs production is very sensitive to variations in the  $\kappa_3$  parameter, reaching deviations of even five orders of magnitude with respect to the SM prediction in the most extreme case ( $\kappa_3 = -10$ ). Similarly to the  $HH$  case, the distance with respect to the SM prediction is approximately constant with energy, and again the peak coming from associated  $Z$  production vanishes as we separate from  $\kappa_3 = 1$ , showing again that the deviations are clearly dominated by WWS.

Figure 4.10 is the equivalent to figure 4.9, this time fixing  $\kappa_3$  to 1 and varying the  $\kappa_4$  parameter. The profile of the deviations is very similar, but softer, being the maximum deviation ( $\kappa_4 = -10$ ) around two orders of magnitude above the SM prediction. As we noted previously, deviations coming from  $ZHHH$  due to  $\kappa_4 \neq 1$  are much smaller than the ones coming from WWS.

We can now look at the dependence with the  $\kappa_3$  and  $\kappa_4$  parameters at a fixed CM energy. Starting with figure 3.8, the main difference that we see when comparing with the results for the subprocess from the previous section is that in this case the highest cross section is always achieved at the highest energy. All cross sections (this is also true for  $HHH$  production) increase with energy and have no peaks at lower energies independently of the value of  $\kappa_3$  or  $\kappa_4$ . The second observation is that there is not a large difference in the sensitivity to  $\kappa_3$  depending on the energy, which is what we meant in the previous paragraphs when saying that the deviations were constant with energy. All the curves experiment a variation between one and two orders of magnitude with respect to the SM in the most extreme case ( $\kappa_3 = -10$ ). All the curves have one minimum, which moves in the region  $\kappa_3 \in [0, 2]$ , being closer to zero at lower energies and closer to two at higher energies.

In figure 3.9 we have the same plot for  $HHH$  production, which exhibits an interesting behaviour, since the two minima that we observed in the equivalent curves for  $W^-W^+ \rightarrow HHH$  subprocess at low values of  $\sqrt{\hat{s}}$  are also manifest in the process. We see two clear minima at  $\sqrt{s} = 380$  GeV, one of them around  $\kappa_3 = 1$  and the other between  $\kappa_3 = 2$  and  $\kappa_3 = 3$ . We also observe and a deformation in the  $\sqrt{s} = 1000, 1500$  and  $3000$  GeV curves, in the region  $\kappa_3 \in [2, 6]$ , apart from the minimum around  $\kappa_3 = 1$ . This deformation does not appear (at least so clearly) in the curve  $\sqrt{s} = 500$  GeV, which only has one minimum around  $\kappa_3 = 1$ . In addition to this, we also notice again how the size of the deviations is comparable for all the energies that we have studied, although much larger than in the  $HH$  case.

Finally, figure 3.10 shows the dependence of  $\sigma(e^-e^+ \rightarrow HHH\nu_e\bar{\nu}_e)$  with  $\kappa_4$  at fixed energies. As we already commented, the deviations are softer in this case. In contrast with the previous plot, in this one the curves exhibit only one minimum, which is around  $\kappa_4 = 1$ . The only curve in which this is not true is the one corresponding to  $\sqrt{s} = 500$

GeV. The cross section at this energy is with difference the least sensible to variations in the  $\kappa_4$  parameter.

Now that we have seen the consequences of varying each of the parameters separately, we can plot the combined effect of varying both at the same time. For reasons that we will motivate later, we will restrict ourselves to study the case of  $\sqrt{s} = 3000$  GeV. The results are shown in figure 4.14, and are consistent with the observations made in the previous plots: the deviations in the cross section are much stronger in the  $\kappa_3$  direction. In addition, sensitivity to  $\kappa_4$  decreases as  $\kappa_3$  distances from one. If we look back to figure 3.11, we notice that, qualitatively, the variations in the cross section of the process at  $\sqrt{s} = 3000$  GeV behave similarly to those of the  $W^-W^+ \rightarrow HHH$  subprocess in the region around  $\sqrt{\hat{s}} = 1000$  GeV. This suggests that the effective energy for WWS in  $e^-e^+$  collisions at  $\sqrt{s} = 3000$  GeV is  $\sqrt{\hat{s}} \sim 1000$  GeV.

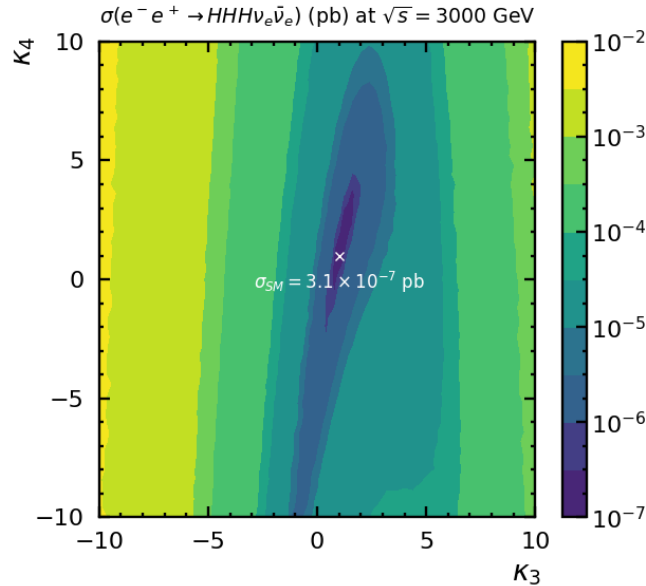


**Figure 4.14:** Contour levels for the total cross section of the  $e^-e^+ \rightarrow HHH\nu_e\bar{\nu}_e$  process represented in the  $(\kappa_3, \kappa_4)$  plane at a CM energy of 3000 GeV. The points have been generated using MADGRAPH 5.

Now that we have characterized both the subprocess and the process for triple Higgs production, we are one step closer to be able to make a prediction, but there is still one ingredient remaining: the collider. In the last part of this section we will consider different possibilities and motivate why our choice of  $\sqrt{s} = 3000$  GeV is the optimal to obtain (if possible) a signal of  $HHH$  production.

#### 4.4 Sensitivity to BSM Higgs self-couplings at $\sqrt{s} = 3000$ GeV

We will focus our forthcoming analysis in the two future linear colliders that are currently on the table, the ILC and CLIC. As we already mentioned in the introduction, they are

both  $e^-e^+$  colliders, and will operate at energies between a few hundredths of GeV and up to 3000 GeV. Each of these energy stages serves a different purpose, being the higher energy configurations the ones oriented to measure the SM triple Higgs self-coupling via SM  $HH$  production, and in principle, none of them is expected to yield a measurable rate regarding SM  $HHH$  production. To illustrate this, tables 4.1 to 4.4 show the cross sections (within the SM) for  $HH$  and  $HHH$  production accompanied by neutrinos ( $\nu\bar{\nu}$ ) and electron neutrinos ( $\nu_e\bar{\nu}_e$ ) and the corresponding number of events for the given integrated luminosity. Note that in both double and triple Higgs production, as we anticipated earlier in this section,  $\sigma(e^-e^+ \rightarrow HH(H)\nu_e\bar{\nu}_e)$  is the dominant contribution within  $\sigma(e^-e^+ \rightarrow HH(H)\nu\bar{\nu})$  at high energies.

Collider	$\sqrt{s}$ (GeV)	$\mathcal{L}_{\text{int}}$ ( $\text{ab}^{-1}$ )	$\sigma(e^-e^+ \rightarrow HH\nu\bar{\nu})$ (pb)	Number of events
ILC	250	2	0	0
	350	0.2	$(8.62 \pm 0.02) \times 10^{-7}$	$< 1$
	500	4	$(3.438 \pm 0.009) \times 10^{-5}$	$137.5 \pm 0.4$
	1000	8	$(9.75 \pm 0.03) \times 10^{-5}$	$780 \pm 2$
CLIC	380	1	$(8.47 \pm 0.02) \times 10^{-6}$	$8.47 \pm 0.02$
	1500	2.5	$(2.416 \pm 0.004) \times 10^{-4}$	$604 \pm 1$
	3000	5	$(8.24 \pm 0.02) \times 10^{-4}$	$4120 \pm 10$

**Table 4.1:** SM cross section and number of events for the process  $e^-e^+ \rightarrow HH\nu\bar{\nu}$  in the different stages of the ILC and CLIC.

Collider	$\sqrt{s}$ (GeV)	$\mathcal{L}_{\text{int}}$ ( $\text{ab}^{-1}$ )	$\sigma(e^-e^+ \rightarrow HH\nu_e\bar{\nu}_e)$ (pb)	Number of events
ILC	250	2	0	0
	350	0.2	$(2.882 \pm 0.008) \times 10^{-7}$	$< 1$
	500	4	$(1.332 \pm 0.003) \times 10^{-5}$	$53.3 \pm 0.1$
	1000	8	$(8.25 \pm 0.02) \times 10^{-5}$	$660 \pm 2$
CLIC	380	1	$(2.875 \pm 0.008) \times 10^{-6}$	$2.875 \pm 0.008$
	1500	2.5	$(2.290 \pm 0.004) \times 10^{-4}$	$573 \pm 1$
	3000	5	$(8.15 \pm 0.02) \times 10^{-4}$	$4080 \pm 10$

**Table 4.2:** SM cross section and number of events for the process  $e^-e^+ \rightarrow HH\nu_e\bar{\nu}_e$  in the different stages of the ILC and CLIC.

Collider	$\sqrt{s}$ (GeV)	$\mathcal{L}_{\text{int}}$ ( $\text{ab}^{-1}$ )	$\sigma(e^-e^+ \rightarrow HHH\nu\bar{\nu})$ (pb)	Number of events
ILC	250	2	0	0
	350	0.2	0	0
	500	4	$(6.95 \pm 0.02) \times 10^{-10}$	$< 1$
	1000	8	$(8.67 \pm 0.02) \times 10^{-8}$	$< 1$
CLIC	380	1	$(5.229 \pm 0.009) \times 10^{-21}$	$< 1$
	1500	2.5	$(9.9 \pm 0.2) \times 10^{-8}$	$< 1$
	3000	5	$(3.340 \pm 0.005) \times 10^{-7}$	$1.670 \pm 0.003$

**Table 4.3:** SM cross section and number of events for the process  $e^-e^+ \rightarrow HHH\nu\bar{\nu}$  in the different stages of the ILC and CLIC.

Collider	$\sqrt{s}$ (GeV)	$\mathcal{L}_{\text{int}}$ ( $\text{ab}^{-1}$ )	$\sigma(e^-e^+ \rightarrow HHH\nu_e\bar{\nu}_e)$ (pb)	Number of events
ILC	250	2	0	0
	350	0.2	0	0
	500	4	$(2.292 \pm 0.007) \times 10^{-10}$	$< 1$
	1000	8	$(3.141 \pm 0.006) \times 10^{-8}$	$< 1$
CLIC	380	1	$(9.62 \pm 0.02) \times 10^{-22}$	$< 1$
	1500	2.5	$(5.145 \pm 0.009) \times 10^{-8}$	$< 1$
	3000	5	$(3.136 \pm 0.007) \times 10^{-7}$	$1.568 \pm 0.004$

**Table 4.4:** SM cross section and number of events for the process  $e^-e^+ \rightarrow HHH\nu_e\bar{\nu}_e$  in the different stages of the ILC and CLIC.

Looking at these tables we understand why the direct measurement of triple Higgs production within the SM is not even suggested. In contrast, we will have a sufficiently large number of events to study SM double Higgs production, specially in the last stage of both colliders. However, since triple Higgs production is about three orders of magnitude less probable, it is not expected to produce more than one event in the best of the situations (CLIC at  $\sqrt{s} = 3000$  GeV), which of course is not enough to perform any study.

Given that these colliders are sensitive to double Higgs production (even if it is SM-like) and therefore this issue has already been studied in detail in the literature, we will now focus our attention in the main topic of this work, which is to study the sensitivity of these experiments to BSM triple Higgs production. We will perform our analysis in the most favourable scenario, which is the last stage of CLIC, at a CM energy of 3000 GeV with an integrated luminosity of  $5 \text{ ab}^{-1}$ . The reason why we choose this configuration is that, as we have seen in our previous calculations, the channel with neutrinos in the final state is the most sensitive to variations of the Higgs self-couplings, and its production cross section grows with energy.

In order to obtain a signal of a particular process, we first need to generate a high enough number of events. Figure 4.15 shows how deviating from  $\kappa_3^{\text{SM}} = 1$  and  $\kappa_4^{\text{SM}} = 1$  can produce a very significant increase in the number of events even if we stay within the most restricting limits given by the experiment,  $\kappa_3 \in [-2.3, 10.3]$  at a 95% CL (there are no constraints on  $\kappa_4$ ).

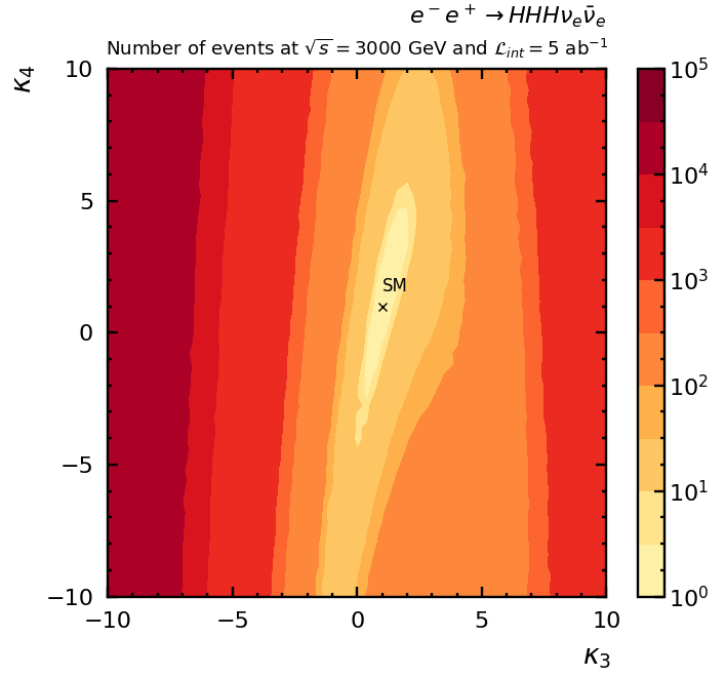


**Figure 4.15:** Contour levels for the number of  $e^- e^+ \rightarrow HHH \nu_e \bar{\nu}_e$  events expected at the last stage of CLIC represented in the  $(\kappa_3, \kappa_4)$  plane.

Now that we have argued that the enhancement in the cross section due to BSM Higgs self-couplings can boost the number of events from one (in the SM) to tens, hundreds or even thousands in the most extreme cases, we can start to think about how this could be detected in the collider. Due to the characteristics of the experiment and of the particles involved, there are several things that will reduce the number of observed events, and must be considered:

- The detector does not cover the whole solid angle, since some space must be left free to place the beam pipe. This means that there will be a number of particles that escape undetected at high values of the pseudorapidity<sup>5</sup>. According to figure 4.16,  $|\eta|_{\text{max}} = 2.72$  in the particular case of CLIC.
- The Higgs boson is not a stable particle. As a consequence, it is not detected directly, but through its decay products. Therefore, the strategy used to select the

<sup>5</sup>Pseudorapidity (also denoted as  $\eta$ ) is a very commonly used spatial coordinate and represents the angle with respect to the beam line, which is usually taken as the  $z$  axis. It is related to the polar angle  $\theta$  by the expression  $\eta = -\log[\tan(\theta/2)]$ .

events depends on the decay channel that we are considering; even if we have a high number of  $HHH$  events, if the branching ratio of the final state that we are looking for is too low, we will run out of statistics. This is why in this work we will opt for using the  $HHH \rightarrow b\bar{b}b\bar{b}b\bar{b}$  decay channel, with a branching ratio of  $0.58^3 \sim 0.2$ , which is the highest of all<sup>6</sup>.

- Regarding the decay channel that we have chosen for our analysis, we also need to take into account the b-jet identification efficiency. Briefly explained, jets coming from b quarks that hadronize can be distinguished from jets coming from gluons or light quarks because they exhibit what is called a secondary vertex. This happens because hadrons containing bottom quarks can travel some distance before decaying to lighter particles that radiate and form the jet itself. We have some control over the b-jet identification efficiency, which has to be balanced with the number of misidentifications that we are willing to accept. This idea is shown in figure 4.17. In this work we will adopt the same value as [48] and take the b-tagging efficiency as 80%. This corresponds to a misidentification efficiency of the 10% for c-jets and the 1% for light flavour jets.
- Finally, it is necessary to characterize the signal to isolate it from the background, which consists on all the processes that can yield a similar final state. Due to the properties of our signal, we will assume that the number of background events that survive after applying all the cuts is negligible. A detailed analysis taking all the backgrounds into account is beyond the scope of this work.

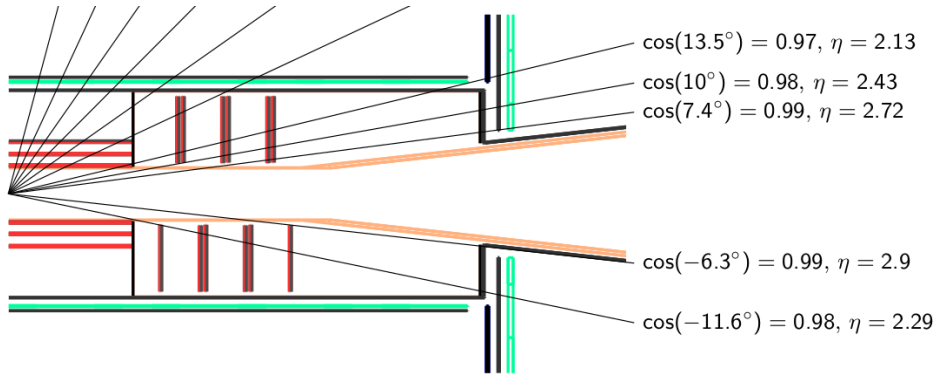


**Figure 4.16:** Illustration of selected angles in the vertex region of the CLIC detector, taken from [47]. The horizontal axis corresponds to the beam line.

<sup>6</sup>It is worth mentioning that other decay channels may be preferred if the number of events allows it due to lower backgrounds or higher precision in the measurement of the final state particles.

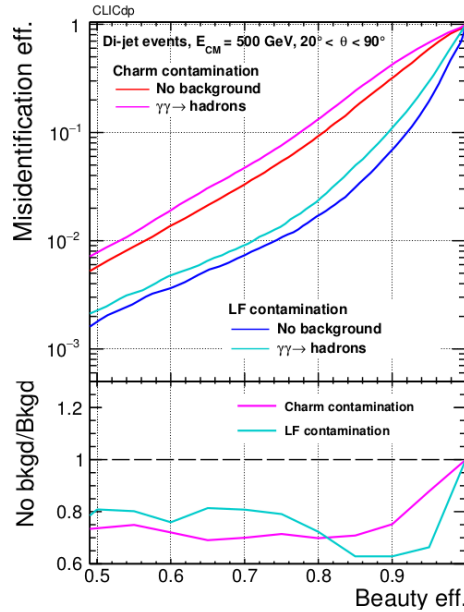


**Figure 4.17:** b-jet identification efficiency, displayed in the horizontal axis, and the corresponding misidentification efficiencies for c-jets and light flavour jets, displayed in the vertical axis. Image taken from [47].

In conclusion, the number of expected events is not  $N = \sigma \mathcal{L}_{\text{int}}$ , but:

$$N_{\text{events}} = N \times \text{BR} \times \varepsilon \times \mathcal{A}, \quad (4.5)$$

where BR is the branching ratio of a particular decay channel,  $\varepsilon$  is the efficiency (here we will only consider the b-tag efficiency) and  $\mathcal{A}$  refers to the fraction of events that pass the kinematical cuts (including those referring to the geometry of the detector). A detailed analysis of  $\varepsilon$  and  $\mathcal{A}$  and all the backgrounds involved would require an independent study and is beyond the scope of this work. However, we can still make an estimation of at least the order of magnitude of  $N_{\text{events}}$  based on what we do know.

Throughout this section we have calculated the cross section of the process of interest, we have chosen a collider with a particular energy and integrated luminosity and we have selected a decay channel for which we know the associated branching ratios and efficiencies. So, what remains is to produce the distributions of the number of events with respect to different kinematic variables in order to narrow down the signal. To do so, we will generate a set of samples for different values of  $\kappa_3$  and  $\kappa_4$  and extrapolate the conclusions to the rest of the  $(\kappa_3, \kappa_4)$  plane. All the events will be generated using MADGRAPH 5 and analyzed using ROOT 6 [49]. Since the hadronization of the b-quarks in the final state is a very expensive task, we will use a resolution criterion instead. Following the reasoning in [48], we will consider an energy resolution  $\Delta E/E = 5\%$  and assume that two quarks with  $\Delta R < 0.4^7$  can not be resolved individually. This condition

<sup>7</sup>The quantity  $\Delta R$  is called angular separation, and can be calculated as  $\Delta R = \sqrt{(\Delta\eta)^2 + (\Delta\phi)^2}$ .

will be applied recursively until we converge to a final list of quarks that we will identify as the (b-)jets.

The following plots show the distributions with respect to several kinematic variables for different values of  $(\kappa_3, \kappa_4)$ . For simplicity we have only plotted deviations of the individual parameters, with the other one set to 1. All histograms are normalized to unity in order to compare their shape.

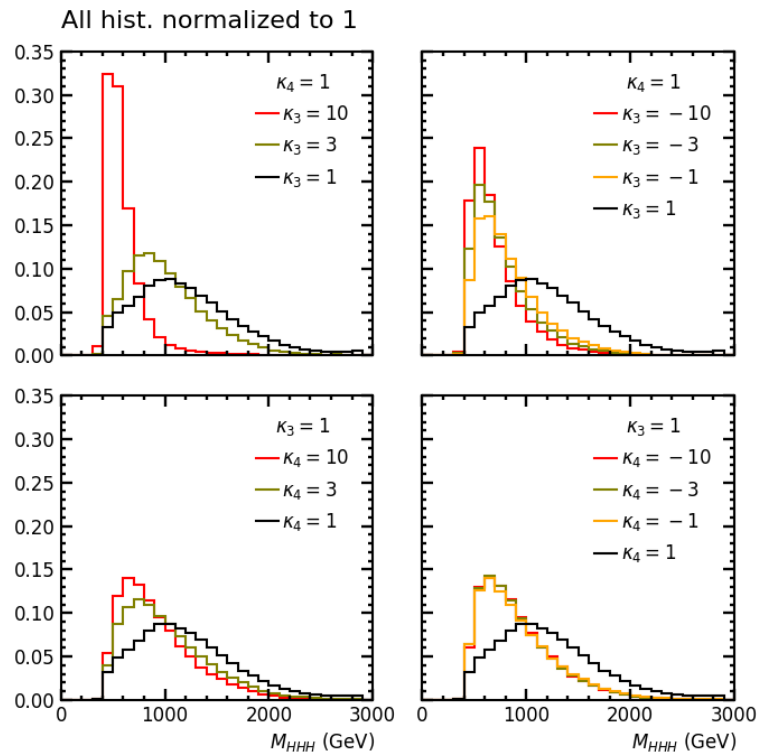


**Figure 4.18:** Distribution of events with the invariant mass of the three Higgs bosons, that is, of the six b-jets.

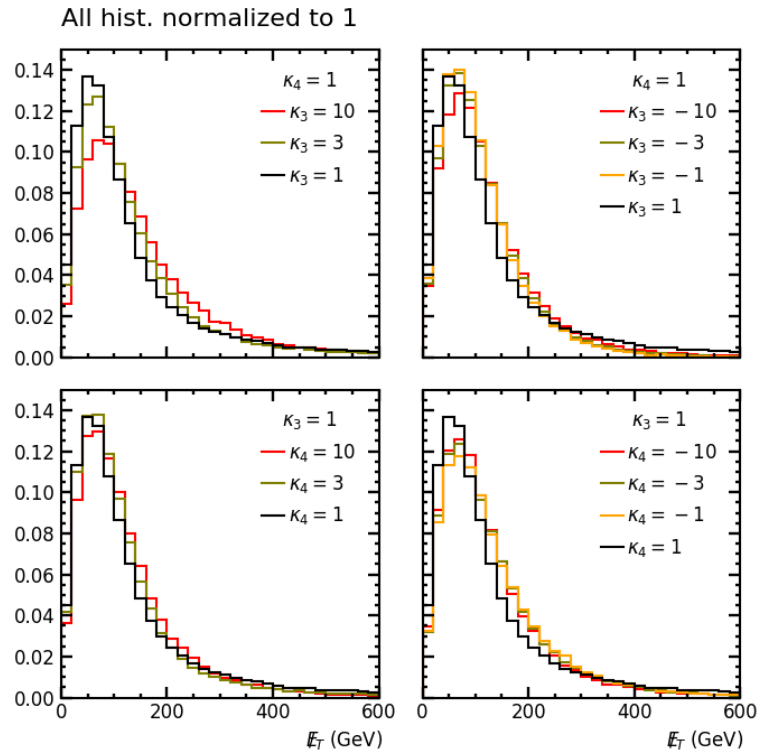


**Figure 4.19:** Distribution of events with the missing transverse energy<sup>8</sup>.

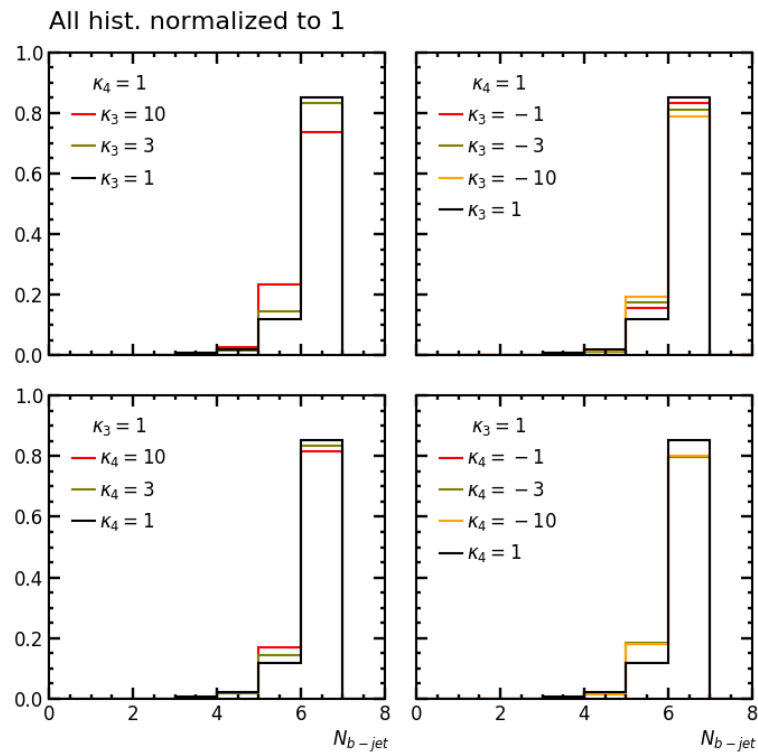


**Figure 4.20:** Distribution of events with the number of b-jets. Note that the number of b-jets is not necessarily six due to the resolution criterion.

<sup>8</sup>In the experiment,  $\vec{E}_T$  is the negative of the vector sum of the transverse momenta of all final state particles reconstructed in the detector, and corresponds to the transverse momentum of all the undetected particles. In our simulation it is computed directly from the transverse momentum of the neutrinos.

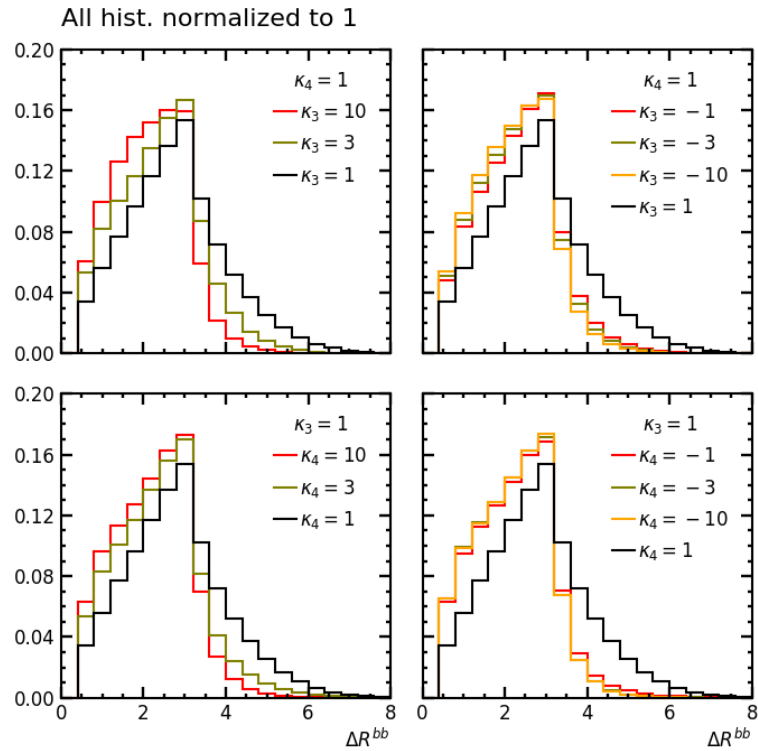


**Figure 4.21:** Distribution of events with the angular separation between b-jets.

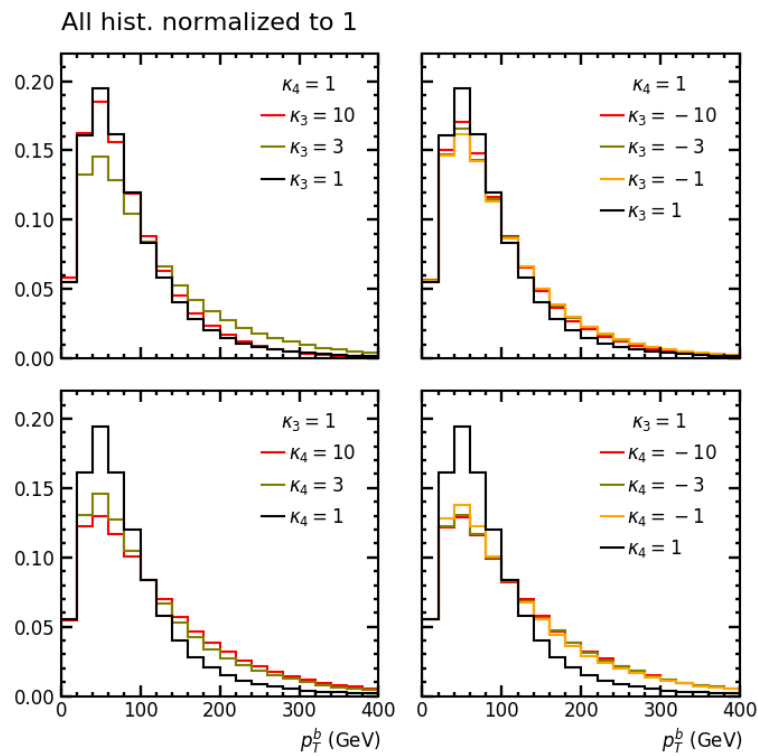


**Figure 4.22:** Distribution of events with the transverse momentum of the b-jets.

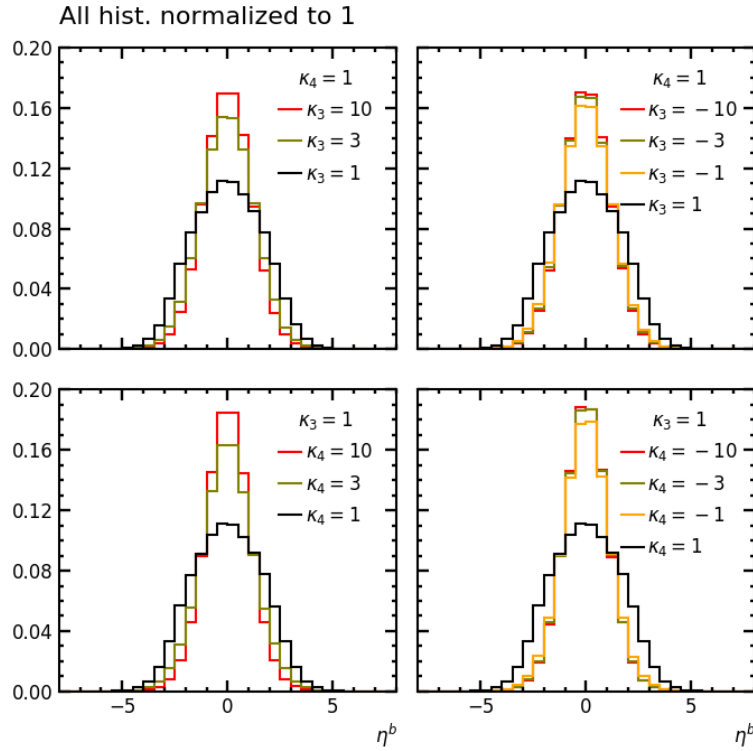


**Figure 4.23:** Distribution of events with the pseudorapidity of the b-jets.

We will not comment each plot one by one, but instead describe some general features. The first thing that we note is that the invariant mass of the  $HHH$ , which is equivalent to  $\sqrt{\hat{s}}$ , is consistent with the observation that we made when comparing figure 4.14 with the corresponding plots for the  $W^-W^+ \rightarrow HHH$  subprocess. In the SM case we see a peak centered around  $M_{HHH} = 1000$  GeV, while for different values of the self-couplings this same peak can be displaced to lower energies, and changes shape. From the  $\cancel{E}_T$  and  $p_T^b$  plots, we also see that both the neutrinos and the b-jets tend to be produced with higher transverse momentum components in BSM scenarios, which is consistent with a smaller value of the pseudorapidity (pseudorapidity of the neutrinos is not showed because it can not be measured in the experiment). As a final remark, we also notice that the number of b-jets decreases as we deviate from the SM. What this means is that the b quarks are produced with smaller relative angles, something that is represented by the variable  $\Delta R^{bb}$ , which is displaced to lower values in the BSM cases.

But as we previously said, the detector does not cover the whole solid angle, but only the region  $|\eta| < 2.72$ . If we restrict to the part of the event that happens within that region, the distributions may (and do) change. Figures 4.18 to 4.23 show a set of variables computed using only the b-jets that fall within the detector. Depending of how optimistic we are, the results can be interpreted in two ways: on the one hand, around 40% of the times at least one b-jet is lost, which means that if we want to identify the six of them we will be rejecting almost half of the events; on the other hand, the BSM distributions

produce b-jets with low pseudorapidity. This implies that in the cases where the cross section can be high enough to perform a measurement, less particles are lost through the beam pipe. The shape of the transverse momentum distributions is not significantly affected by this cut.

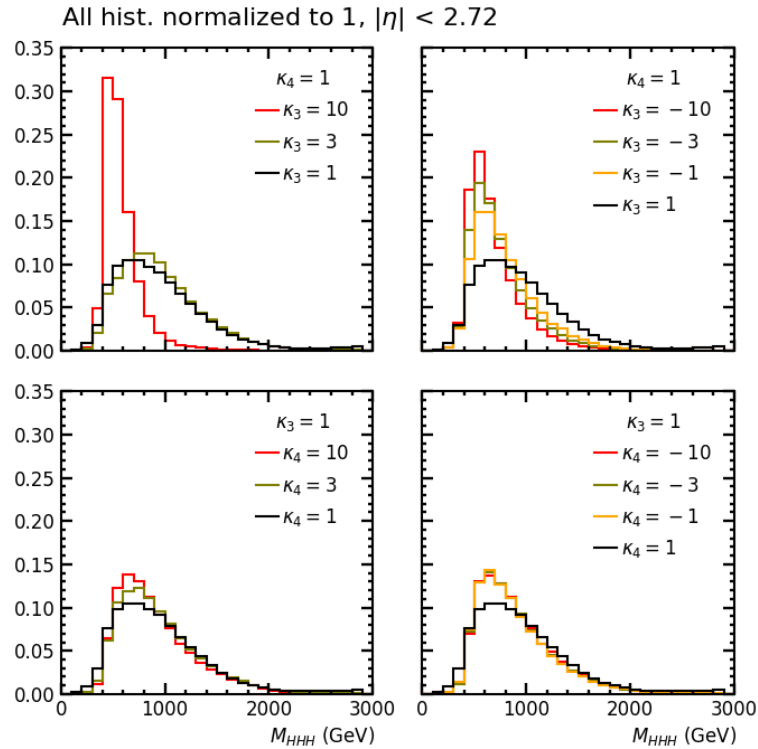


**Figure 4.24:** Distribution of events with the invariant mass of the three Higgs bosons after applying the cut  $|\eta| < 2.72$

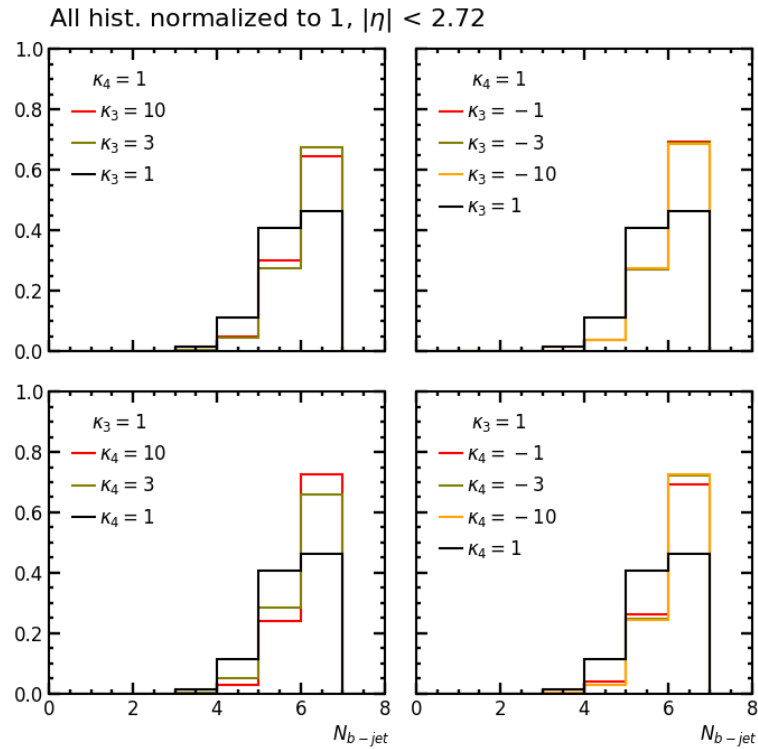


**Figure 4.25:** Distribution of events with the number of b-jets after applying the cut  $|\eta| < 2.72$

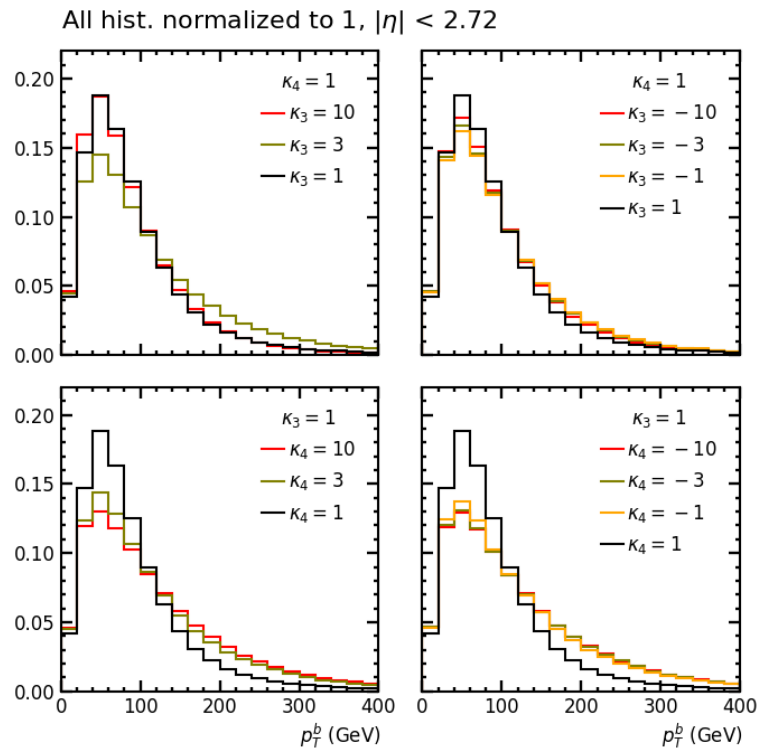


**Figure 4.26:** Distribution of events with the transverse momentum of the b-jets after applying the cut  $|\eta| < 2.72$

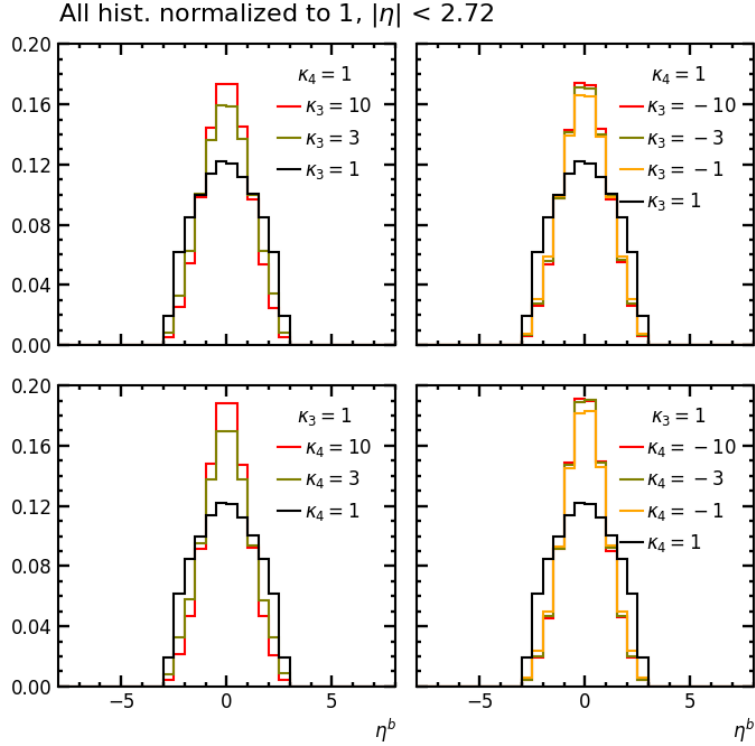


**Figure 4.27:** Distribution of events with the pseudorapidity of the b-jets after applying the cut  $|\eta| < 2.72$

Now that we know the shape of a set of relevant distributions, we will impose some additional cuts based on [48] but slightly modified, including a requirement that the event reaches a minimum value of the missing transverse energy:

$$\begin{aligned}
 N_{\text{jet}} &\geq 6, \\
 p_T^{\text{jet}} &\geq 20 \text{ GeV}, \\
 N_{\text{b-jet}} &\geq 5, \\
 \cancel{E}_T &\geq 20 \text{ GeV}.
 \end{aligned}
 \tag{4.6}$$

First of all, we require our events to have six jets. Note that in our simulations we know that the jets are coming from b-quarks, but in an experiment this is unknown a priori. We also impose that these jets have a minimum transverse momentum of 20 GeV, since very low  $p_T$  jets can be difficult to detect. Next, we want at least five jets to be identified as b-jets. The reason why we do not require 6 tagged b-jets lies on the efficiency. Assuming that all jets are equal, i.e., that they are not sorted or classified in any way, the probability of identifying five out of the six as b-jets is:

$$\varepsilon_5 = 6 \times 0.8^5 \times 0.2 + 0.8^6 = 0.66,
 \tag{4.7}$$

while if we tag the six of them:

$$\varepsilon_6 = 0.8^6 = 0.26, \quad (4.8)$$

so allowing five tagged jets is way more efficient. It is important to note that since all b-jets come from on-shell Higgs bosons, the three pairs should reconstruct the Higgs invariant mass. Although the resolution will not be very good since we are treating with jets, this could be an additional cut to reject backgrounds. The last condition in the list is to have missing transverse energy to ensure that we are looking at events which contain neutrinos in the final state. The value of  $\mathcal{A}$  after applying all these cuts is approximately between 0.44 and 0.51, although it drops to 0.34 at  $\kappa_3 = \kappa_4 = 1$ . To compute the number of observed events we will use the following values:

$$N_{\text{events}} = N \times 0.58^3 \times (6 \times 0.8^5 \times 0.2 + 0.8^6) \times 0.48,$$

where  $\mathcal{A}$  is given by an average and takes the same value in all cases. The results can be seen in figure 4.28.

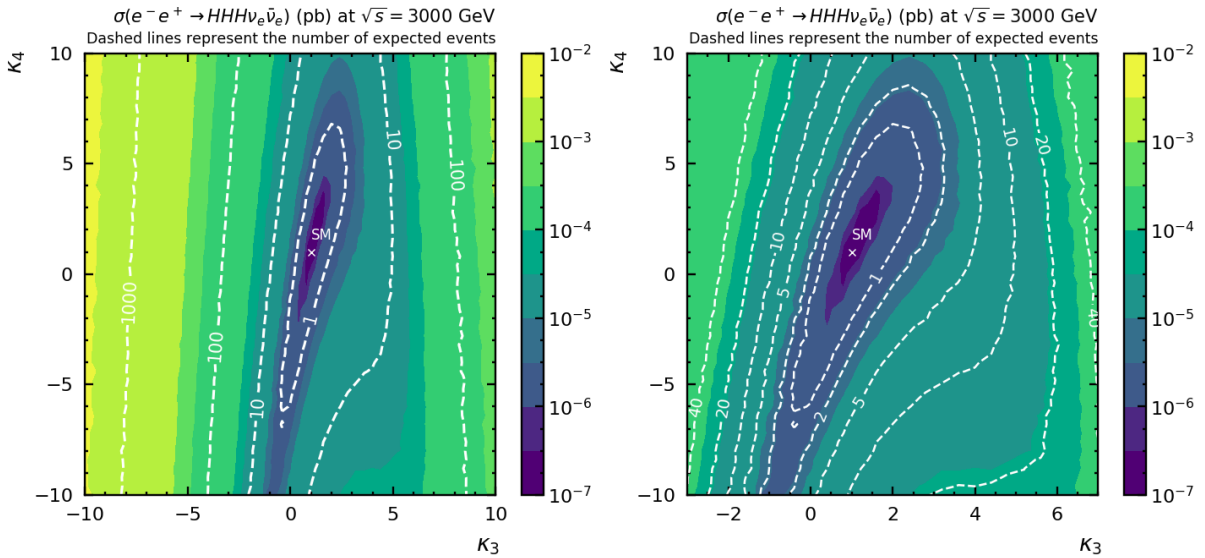


**Figure 4.28:** Contour lines for the number of  $e^-e^+ \rightarrow b\bar{b}b\bar{b}b\bar{b}\nu_e\bar{\nu}_e$  expected events (white dashed line) after applying all the cuts, represented in the  $(\kappa_3, \kappa_4)$  plane. The corresponding  $e^-e^+ \rightarrow HHH\nu_e\bar{\nu}_e$  cross section is also shown for comparison. The right plot shows a closer view in the  $\kappa_3$  axis.

If we set a minimum value for the number of observed events such as  $N_{\text{obs}} = 10$ , we find that we are sensitive to a significant fraction of the  $(\kappa_3, \kappa_4)$  plane. Even if we exclude the region  $\kappa_3 \in [-2.3, 10.3]$ , there are still many values of  $\kappa_3$  and  $\kappa_4$  that would produce a visible signal if we assume that the background is negligible. This is represented in figure 4.29.

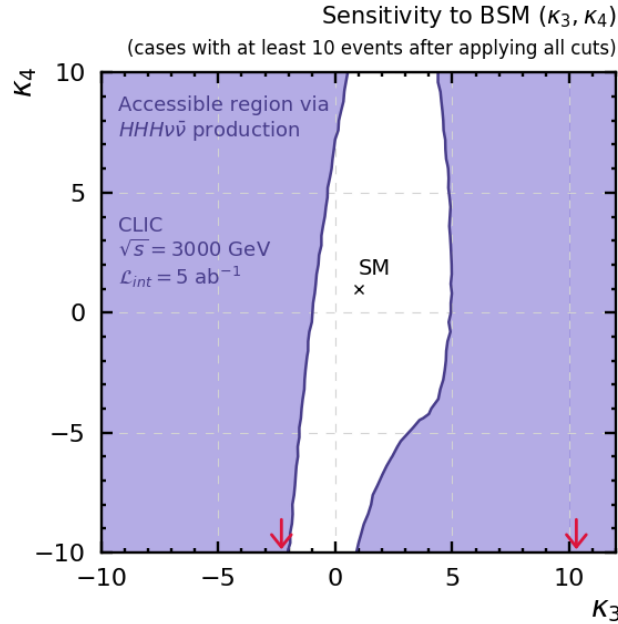


**Figure 4.29:** Accessible region in the  $(\kappa_3, \kappa_4)$  plane of BSM scenarios to triple Higgs production via  $e^-e^+ \rightarrow HHH\nu\bar{\nu}$  at  $\sqrt{s} = 3000$  GeV and  $\mathcal{L}_{\text{int}} = 5 \text{ ab}^{-1}$ . The red arrows mark the limits of the present bound from ATLAS [19] for  $\kappa_3$ , given in eq. 2.19.

## 5 Conclusions

The Standard Model of particle physics can be regarded as a very successful theory; over the last decades, its predictions have led to very relevant discoveries in the field, culminating with the measurement of a scalar compatible with the SM Higgs boson in 2012 at the LHC. However, there are both experimental evidence and theoretical problems which are not covered in the SM and make us think that the theory is still incomplete.

Throughout this work we have focused our attention in the Electroweak Symmetry Breaking Sector of the SM, and in particular, in the Brout-Englert-Higgs mechanism, which postulates how the spontaneous breaking of the  $SU(2)_L \times U(1)_Y$  gauge symmetry by a scalar doublet  $\Phi$  generates the masses of the  $W^\pm$  and  $Z$  bosons, and allows to define gauge invariant mass terms for the fermions (except for neutrinos). The Higgs boson appears in the SM thanks to this mechanism, but although it solves several disagreements between the theory and the experiment, such as the non-vanishing particle masses or unitarity violation of longitudinal vector boson scattering, it also raises some questions. For example, why is there only one scalar fundamental particle in the SM? Why is it embedded in a doublet? Why is its mass so small?

There is not a unique answer to these questions; through the years, many UV theories have been proposed to explain the origin of the BEH mechanism in a more satisfactory

way. Some of them introduce new symmetries that are broken at the scales that we can probe, while others consider the possibility that the Higgs boson is a composite state. What is clear is that it is not efficient to test them individually, reason why effective field theories are a powerful tool; since they allow to parametrize deviations from the SM in a very generic way, they can be used to examine several models at once.

The Electroweak Chiral Lagrangian is an example of an EFT inspired in the QCD Chiral Lagrangian; as we have seen, the Goldstone bosons are introduced in this Lagrangian in a non-linear representation, while the Higgs boson is a singlet described by a polynomial function. This formulation allows us to introduce independent BSM Higgs self-couplings, in contrast to the theories in which the Higgs boson is embedded in a doublet. Moreover, since the EChL is not linked to any particular high energy completion, the deviations parametrized in this way can then be interpreted in terms of different UV theories.

Using this effective theory we have studied BSM deviations coming from the Higgs self-couplings in the  $W^-W^+ \rightarrow HHH$  subprocess. The results obtained show that its cross section is much more sensitive to variations in the triple self-coupling ( $\kappa_3 \neq \kappa_3^{\text{SM}} = 1$ ) than  $\sigma(W^-W^+ \rightarrow HH)$  without violating unitarity within the region that we are exploring. Since the quartic coupling is also involved in the calculation of  $\sigma(W^-W^+ \rightarrow HHH)$ , this cross section is in addition sensitive to deviations in  $\kappa_4$ , which is a very significant difference with respect to double Higgs production. Again, the range of values of  $\kappa_4$  that we have considered do not lead to unitarity violation in the energy interval that we have considered, that is, up to 3000 GeV.

In order to study the whole process, that is, multiple Higgs production coming from  $e^-e^+$  collisions, we have focused on  $HH$  and  $HHH$  production with neutrinos in the final state, that is,  $\sigma(e^-e^+ \rightarrow HH\nu\bar{\nu})$  and  $\sigma(e^-e^+ \rightarrow HHH\nu\bar{\nu})$ , and in particular  $\sigma(e^-e^+ \rightarrow HH\nu_e\bar{\nu}_e)$  and  $\sigma(e^-e^+ \rightarrow HHH\nu_e\bar{\nu}_e)$ , which constitute, respectively, the dominant  $HH$  and  $HHH$  production mechanisms at high energies. The study of the subprocesses is relevant here because these cross sections have an important contribution coming from WWS diagrams, which becomes more significant as we increase the CM energy,  $\sqrt{s}$ .

In this work we have considered two approaches; first, we have used the effective  $W$  approximation, a factorization which assumes that the  $W$  bosons are radiated from the electrons following a distribution function and then scatter on-shell. The plots generated using this approximation show that the accuracy in triple Higgs production is worse than in double Higgs production, and therefore it should not be used to obtain precise numerical results. The estimate of the  $e^-e^+ \rightarrow HHH\nu_e\bar{\nu}_e$  cross section provided by this approximation differs by about a factor of two with respect to the exact result. This is in contrast to the  $HH\nu_e\bar{\nu}_e$  case, where we have checked that the EWA provides a very

accurate result. However, it is still useful to understand how WWS takes place, and how longitudinal  $WW$  scattering is the dominant contribution to the cross section. The other method that we have used to produce the results is Monte Carlo simulation of the full process. In this case we have seen that  $\sigma(e^-e^+ \rightarrow HHH\nu\bar{\nu})$  is much more sensitive to  $\kappa_3$  than  $\sigma(e^-e^+ \rightarrow HH\nu\bar{\nu})$  as we expected from the results obtained for the subprocess. The sensitivity to  $\kappa_4$  in  $\sigma(e^-e^+ \rightarrow HHH\nu_e\bar{\nu}_e)$  is smaller compared to  $\kappa_3$ , but still significant in certain regions of the  $(\kappa_3, \kappa_4)$  plane. Notice that  $\kappa_4$  does not enter in the calculation of the  $e^-e^+ \rightarrow HH\nu_e\bar{\nu}_e$  cross section, and therefore triple Higgs production is the only channel sensitive to  $\kappa_4$ .

To obtain a more realistic representation of what should be expected from triple Higgs production in the experiment, in the last part of this work we have chosen a collider (CLIC at  $\sqrt{s} = 3000$  GeV and  $\mathcal{L}_{\text{int}}$ ) and a decay channel ( $HHH \rightarrow b\bar{b}b\bar{b}b\bar{b}$ ) and we have implemented a set of kinematical cuts to reduce possible backgrounds, which we have assumed to be very low due to the characteristic signature of the signal. The results show that a considerable fraction of the  $(\kappa_3, \kappa_4)$  plane will be accessible at CLIC, with 10 or more expected events in the detector. In the case that the Higgs self-couplings are sufficiently far from the SM, triple Higgs production could nicely complement the study of  $\kappa_3$  via double Higgs production, and also provide new information about  $\kappa_4$ .

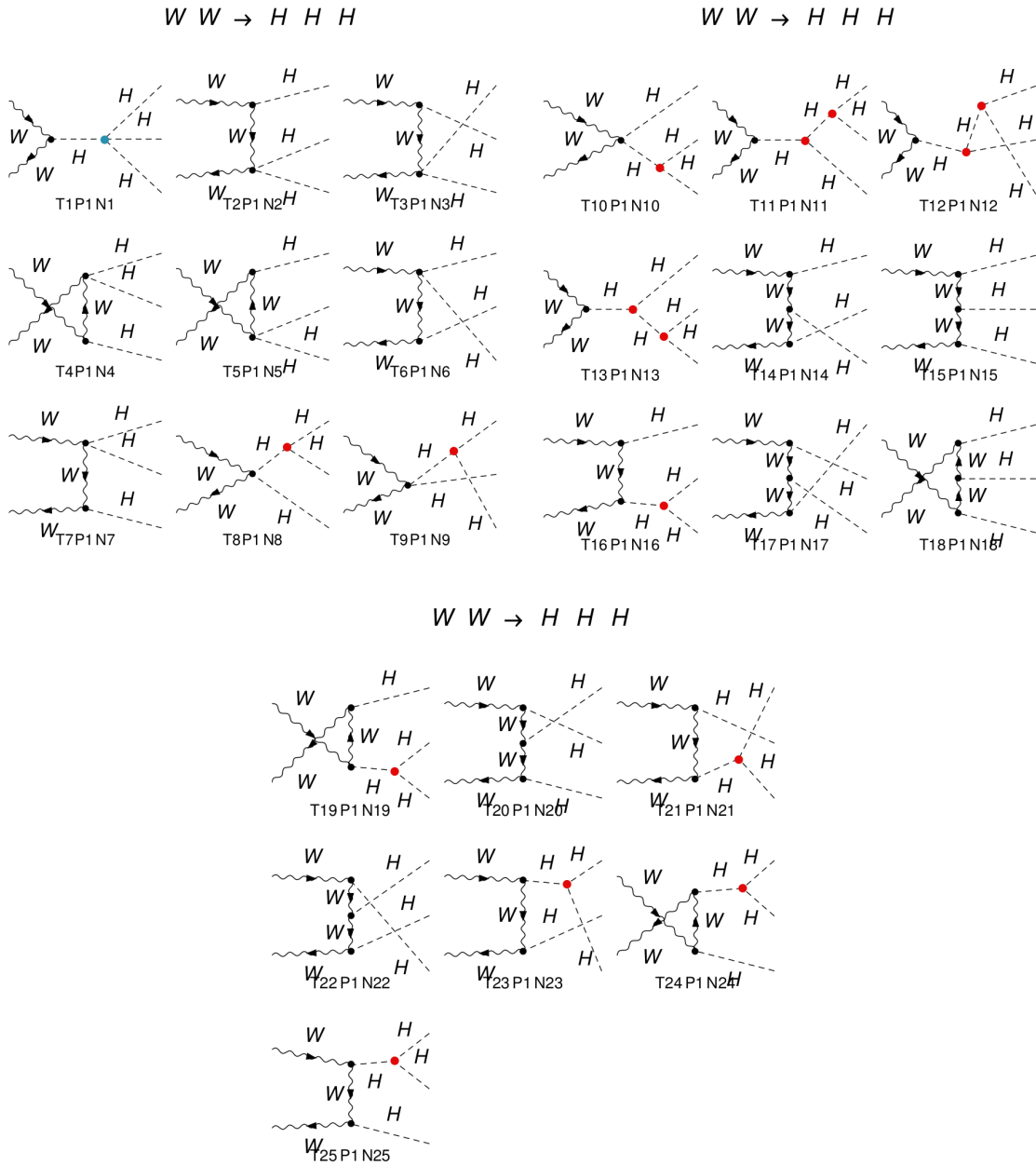
In summary, we have introduced the EChL to be able to study the BSM physics using an effective theory, and to define the parameters that characterize the deviations in the triple and quartic Higgs boson self-couplings. We have analyzed the  $W^-W^+ \rightarrow HHH$  subprocess, both within the SM and beyond, and compared it with  $W^-W^+ \rightarrow HH$ . Then, we have tested the validity of the effective  $W$  approximation for triple Higgs production (in addition to double Higgs production) in an  $e^-e^+$  collider, and finally we have used Monte Carlo simulation to evaluate the deviations in  $HHH\nu\bar{\nu}$  production induced by BSM Higgs self-couplings and give an approximate result for the region of the  $(\kappa_3, \kappa_4)$  plane in which CLIC would be sensitive to those deviations. The results are promising, since they suggest that triple Higgs production via  $HHH\nu\bar{\nu}$  could be accessible at CLIC, offering the possibility of studying (or constraining) the triple and quartic Higgs self-couplings at the same time.

# Appendix

fu

## I Diagrams contributing to $W^-W^+ \rightarrow HHH$

The following diagrams have been generated using FEYNARTS-3.10 in the unitary gauge. These are the diagrams used to compute  $\sigma(W^-W^+ \rightarrow HHH)$ , using FORMCALC-9.6 to perform the analytical calculation of the corresponding amplitude (see next appendix), and VEGAS to integrate over the phase space. The red and blue dots represent the triple and quartic Higgs self-interactions, respectively.



## II Analytic expression for the $W^-W^+ \rightarrow HHH$ amplitude

The following amplitude for the subprocess  $W^-W^+ \rightarrow HHH$  has been generated using FEYNARTS-3.10 and FORMCALC-9.6.

$$\mathcal{M}(W^-W^+ \rightarrow HHH) =$$

$$\begin{aligned} & \frac{1}{\text{SW SW2}} \text{Alfa EL } \pi \left( \text{Pair1} \left( 3 \text{MH2} \left( \frac{\text{MW Den[S, MH2]}}{\text{MW2}} + \frac{\text{Den[S34, MH2]}}{\text{MW}} \right) + \right. \right. \\ & \quad \left. \frac{1}{\text{MW}} \left( 9 \text{MH2}^2 \text{Den[S, MH2] Den[S34, MH2]} + \left( 3 \text{MH2} + 9 \text{MH2}^2 \text{Den[S, MH2]} \right) \right. \right. \\ & \quad \left. \left. \left( \text{Den[4 MH2 + 2 MW2 - S34 - T14 - T24, MH2]} + \text{Den[4 MH2 + 2 MW2 - S34 - T - U, MH2]} \right) \right) \right) + \\ & \text{MW} \left( 2 \left( \left( \text{Pair1} + \frac{\text{Abb5 Pair6}}{\text{MW2}} \right) \text{Den[T, MW2]} + \left( \text{Pair1} + \frac{\text{Abb2 Pair3}}{\text{MW2}} \right) \text{Den[3 (MH2 + MW2) - S -} \right. \right. \\ & \quad \left. \left. \text{T - T14, MW2]} + \left( \text{Pair1} + \frac{\text{Abb9 Pair9}}{\text{MW2}} \right) \text{Den[T14, MW2]} \right) + \left( 2 \left( \text{Pair1} + \frac{\text{Abb15 Pair8}}{\text{MW2}} \right) - \right. \\ & \quad \left. 2 \left( \text{Sub3 Den[T, MW2]} + \text{Sub5 Den[3 (MH2 + MW2) - S - T - T14, MW2]} \right) \right) \text{Den[T24, MW2]} + \\ & \quad 6 \text{MH2} \left( \left( \text{Pair1} + \frac{\text{Abb2 Pair3}}{\text{MW2}} \right) \text{Den[S34, MH2] Den[3 (MH2 + MW2) - S - T - T14, MW2]} + \right. \\ & \quad \left( \text{Pair1} + \frac{\text{Abb5 Pair6}}{\text{MW2}} \right) \text{Den[T, MW2] Den[4 MH2 + 2 MW2 - S34 - T14 - T24, MH2]} + \\ & \quad \left. \left( \left( \text{Pair1} + \frac{\text{Abb9 Pair9}}{\text{MW2}} \right) \text{Den[T14, MW2]} + \left( \text{Pair1} + \frac{\text{Abb15 Pair8}}{\text{MW2}} \right) \text{Den[T24, MW2]} \right) \right. \\ & \quad \left. \text{Den[4 MH2 + 2 MW2 - S34 - T - U, MH2]} \right) + \\ & \quad \left( \left( \text{Pair1} + \frac{\text{Abb1 Pair4}}{\text{MW2}} \right) (2 + 6 \text{MH2 Den[S34, MH2]}) - \right. \\ & \quad \left. 2 \left( \text{Sub1 Den[T, MW2]} + \text{Sub2 Den[T14, MW2]} \right) \right) \text{Den[3 (MH2 + MW2) - S - T24 - U, MW2]} + \\ & \quad \left( -2 \left( \text{Sub6 Den[3 (MH2 + MW2) - S - T - T14, MW2]} + \text{Sub4 Den[T14, MW2]} \right) + \left( \text{Pair1} + \right. \right. \\ & \quad \left. \left. \frac{\text{Abb17 Pair7}}{\text{MW2}} \right) (2 + 6 \text{MH2 Den[4 MH2 + 2 MW2 - S34 - T14 - T24, MH2]}) \right) \text{Den[U, MW2]} \Big) \end{aligned}$$

Here SW (SW2) is the sine of the weak angle (squared), Alfa is the fine-structure constant and EL is the electron charge magnitude. The masses (squared) of the Higgs and  $W$  bosons are represented as MH (MH2) and MW (MW2). The rest of the definitions are shown in table II.1. We will refer to the 4-momentum vectors of the  $W^-$  and  $W^+$  bosons as  $k_1$  and  $k_2$ , respectively, and we will denote their corresponding polarization vectors as  $\epsilon_1$  and  $\epsilon_2$ . The 4-momentum vectors of the three Higgs bosons are denoted as  $k_3$ ,  $k_4$  and  $k_5$ , respectively.

Den[a, b]	$1/(a-b)$
Pair1	$\epsilon_1 \cdot \epsilon_2$
Pair2	$\epsilon_1 \cdot k_2$
Pair3	$\epsilon_1 \cdot k_5$
Pair4	$\epsilon_2 \cdot k_5$
Pair5	$\epsilon_2 \cdot k_1$
Pair6	$\epsilon_1 \cdot k_3$
Pair7	$\epsilon_2 \cdot k_3$
Pair8	$\epsilon_2 \cdot k_4$
Pair9	$\epsilon_1 \cdot k_4$
S	$(k_1 + k_2)^2 = \hat{s}$
S34	$(k_3 + k_4)^2$
T	$(k_1 - k_3)^2$
T14	$(k_1 - k_4)^2$
T24	$(k_2 - k_4)^2$
U	$(k_2 - k_3)^2$
Abb1	Pair2 - Pair3
Abb2	-Pair4 + Pair5
Abb3	(Pair2 - Pair3)Pair4 + Pair6(Pair5 - Pair7)
Abb4	Pair4 Pair6(-3MH2 - MW2 + S34 + 2T + T14)
Abb5	Pair5 - Pair7
Abb6	Pair6 Pair8(-MH2 + T + T24)
Abb7	Pair6(Pair5 - Pair7) + Pair8(Pair2 - Pair9)
Abb8	(Pair2 - Pair3)Pair4 + (Pair5 - Pair8)Pair9
Abb9	Pair5 - Pair8
Abb10	Pair4 Pair9(-3MH2 - MW2 + S34 + T + 2T14)
Abb11	(Pair2 - Pair6)Pair7 + (Pair5 - Pair8)Pair9
Abb12	Pair7 Pair9(-MH2 + T14 + U)
Abb13	Pair3(-Pair4 + Pair5) + Pair8(Pair2 - Pair9)
Abb14	Pair3 Pair8(-3MH2 - MW2 + S34 + 2T24 + U)
Abb15	Pair2 - Pair9
Abb16	Pair3 Pair7(-3MH2 - MW2 + S34 + T24 + 2U)
Abb17	Pair2 - Pair6
Abb18	Pair3(-Pair4 + Pair5) + (Pair2 - Pair6)Pair7
Sub1	Abb4/MW2 - 2(Abb3 + MW2 Pair1)
Sub2	Abb10/MW2 - 2(Abb8 + MW2 Pair1)
Sub3	Abb6/MW2 - 2(Abb7 + MW2 Pair1)
Sub4	Abb12/MW2 - 2(Abb11 + MW2 Pair1)
Sub5	Abb14/MW2 - 2(Abb13 + MW2 Pair1)
Sub6	Abb16/MW2 - 2(Abb18 + MW2 Pair1)

**Table II.1:** Parameters, abbreviations and subexpressions generated by FORMCALC-9.6.

### III Variable redefinition for VEGAS numerical integration

Monte Carlo integration is a method for numerical integration that allows to compute definite integrals using (pseudo)random numbers and is particularly useful when we need to integrate over multiple variables, as it is our case. This is done in Python using the VEGAS module. In order to optimize the performance of the code, we define all of our variables from 0 to 1, so that they are independent and cover the same interval. This is done in both the cross section of the subprocess and the EWA, but since the first is contained within the second, we will use the EWA  $\sigma(e^-e^+ \rightarrow HH(H)\nu_e\bar{\nu}_e)$  cross section from section 4 (equation 4.4) to illustrate the changes of variables that we need to do.

The expression that we need to compute in this case is:

$$\sigma(s) = \int dx_1 \int dx_2 \frac{1}{3!} \frac{1}{2\sqrt{\hat{s}^2 - 4\hat{s}m_W^2}} \frac{1}{32(2\pi)^4\hat{s}} \int dm_{34}^2 \int dm_{45}^2 \int d\cos\theta_3 \int d\phi_{35} \sum_{i,j} f_i(x_1)f_j(x_2)|\overline{\mathcal{M}}_{ij}|^2, \quad (\text{III.1})$$

so we start by introducing two new variables,  $\tau$  and  $\eta$

$$\begin{aligned} \tau &\equiv x_1x_2 \quad \text{from} \quad \frac{\hat{s}_{\min}}{s} \quad \text{to} \quad \frac{\hat{s}_{\max}}{s}, \\ \eta &\equiv \frac{1}{2} \log \frac{x_1}{x_2} \quad \text{from} \quad \log \sqrt{\tau} \quad \text{to} \quad -\log \sqrt{\tau}. \end{aligned} \quad (\text{III.2})$$

To guarantee that the three Higgs bosons are produced on-shell,  $\hat{s}_{\min} = (3m_H)^2$ , while  $\hat{s}_{\max} = s$ . The condition that the  $W$  bosons are also on-shell (required when computing the cross section of the subprocess and also a condition of the EWA) is implicit in the distribution functions, which go to zero when their energy is below  $m_W$ . This is the same as imposing that:

$$f_i(x) = 0 \quad \text{when} \quad x < \frac{2m_W}{\sqrt{s}}, \quad (\text{III.3})$$

since each initial fermion carries an energy  $E = \sqrt{s}/2$ . The jacobian determinant of this change of variables is equal to 1, so the new integral reads:

$$\sigma(s) = \int d\tau \int d\eta \frac{1}{3!} \frac{1}{2\sqrt{(\tau s)^2 - 4\tau sm_W^2}} \frac{1}{32(2\pi)^4\tau s} \int dm_{34}^2 \int dm_{45}^2 \int d\cos\theta_3 \int d\phi_{35} \sum_{i,j} f_i[x_1(\tau, \eta)]f_j[x_2(\tau, \eta)] |\overline{\mathcal{M}}_{ij}|^2, \quad (\text{III.4})$$

where  $x_1(\tau, \eta) = \sqrt{\tau}e^\eta$  and  $x_2(\tau, \eta) = \sqrt{\tau}e^{-\eta}$ . This transformation does not make the integration limits independent, but allow us to define the variables that we are going to

use in the final calculation. As we said before, we normalize them such that they all vary from 0 to 1:

$$\begin{aligned}
\omega_0 &\equiv \frac{\tau - \tau_{\min}}{\tau_{\max} - \tau_{\min}}, & \tau &= (\tau_{\max} - \tau_{\min})\omega_0 + \tau_{\min}, \\
\omega_1 &\equiv \frac{1}{2} \left( 1 - \frac{\eta}{\log \sqrt{\tau}} \right), & \eta &= (1 - 2\omega_1) \log \sqrt{\tau}, \\
\omega_2 &\equiv \frac{\log(m_{34}^2/m_{34,\min}^2)}{\log(m_{34,\max}^2/m_{34,\min}^2)}, & m_{34}^2 &= m_{34,\min}^2 \exp \left( \omega_2 \log \frac{m_{34,\max}^2}{m_{34,\min}^2} \right), \\
\omega_3 &\equiv \frac{\log(m_{45}^2/m_{45,\min}^2)}{\log(m_{45,\max}^2/m_{45,\min}^2)}, & m_{45}^2 &= m_{45,\min}^2 \exp \left( \omega_3 \log \frac{m_{45,\max}^2}{m_{45,\min}^2} \right), \\
\omega_4 &\equiv \frac{1}{2}(1 + \cos \theta_3), & \cos \theta_3 &= 2\omega_4 - 1, \\
\omega_5 &\equiv \frac{\phi_{35}}{2\pi}, & \phi_{35} &= 2\pi\omega_5.
\end{aligned} \tag{III.5}$$

The jacobian determinant is not trivial in this case, but it can be easily calculated:

$$J(\vec{\omega}) = 4\pi \left| (1 - \tau_{\min}) 2 \log \sqrt{\tau} m_{34}^2 \log \frac{m_{34,\max}^2}{m_{34,\min}^2} m_{45}^2 \log \frac{m_{45,\max}^2}{m_{45,\min}^2} \right|. \tag{III.6}$$

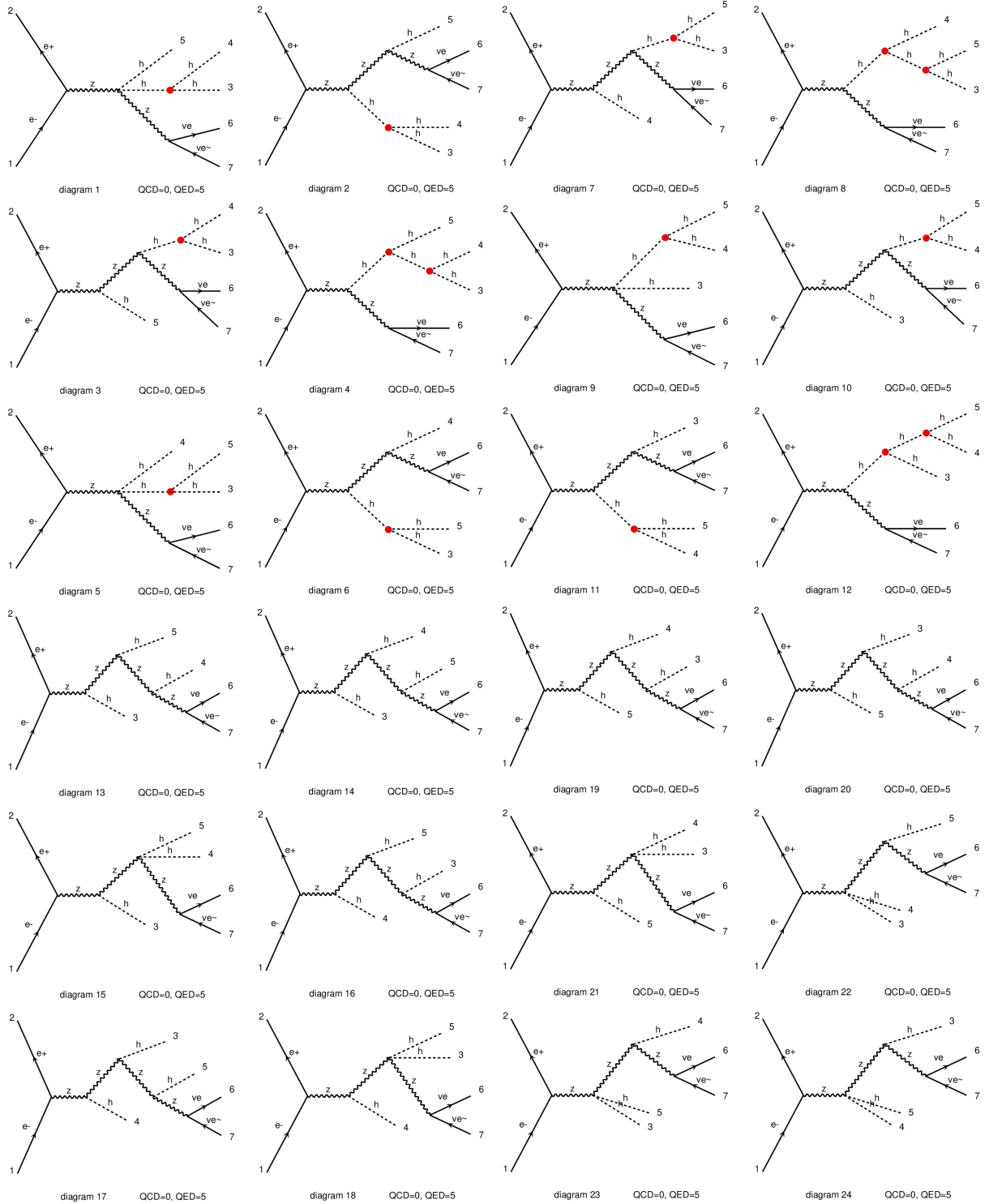
The dependence on  $\vec{\omega} = (\omega_0, \omega_1, \omega_2, \omega_3, \omega_4, \omega_5)$  is given by III.5. After substituting the old variables by  $\vec{\omega}$ , the resulting integral is:

$$\begin{aligned}
\sigma(s) &= \int_0^1 d\omega_0 \int_0^1 d\omega_1 \int_0^1 d\omega_2 \int_0^1 d\omega_3 \int_0^1 d\omega_4 \int_0^1 d\omega_5 \\
&\quad \frac{1}{3!} \frac{1}{2\sqrt{(\tau(\omega_0)s)^2 - 4\tau(\omega_0)sm_W^2}} \frac{1}{32(2\pi)^4\tau(\omega_0)s} J(\vec{\omega}) \\
&\quad \sum_{i,j} f_i(x_1[\tau(\omega_0), \eta(\omega_0, \omega_1)]) f_j(x_2[\tau(\omega_0), \eta(\omega_0, \omega_1)]) |\overline{\mathcal{M}}_{ij}|^2,
\end{aligned} \tag{III.7}$$

which can be integrated numerically.

## IV Diagrams contributing to $e^-e^+ \rightarrow HHH \nu_e \bar{\nu}_e$

The following diagrams have been generated using MADGRAPH 5 in the unitary gauge. These are the diagrams used to compute  $\sigma(e^-e^+ \rightarrow HHH \nu_e \bar{\nu}_e)$  using Monte Carlo simulation. The red and blue dots represent the triple and quartic Higgs self-interactions, respectively. Diagrams 1 to 25 are  $Z$ -mediated, while diagrams 26 to 50 correspond to WWS.





## References

- [1] S.L. Glashow, *Partial-symmetries of weak interactions*, Nucl. Phys. **22** (1961) 4
- [2] M. Gell-Mann, *A schematic model of baryons and mesons*, Phys. Lett. **8** (1964) 3
- [3] S. Weinberg, *A model of leptons*, Phys. Rev. Lett. **19** (1967) 1264
- [4] A. Salam, *Weak and electromagnetic interactions*, Conf. Proc. **C680519** (1968) 367
- [5] P.W. Higgs, *Broken symmetries, massless particles and gauge fields*, Phys. Lett. **12** (1964) 2
- [6] P.W. Higgs, *Broken symmetries and the masses of gauge bosons*, Phys. Rev. Lett. **13** (1964) 508
- [7] F. Englert and R. Brout, *Broken symmetry and the mass of gauge vector mesons*, Phys. Rev. Lett. **13** (1964) 321
- [8] G.S. Guralnik, C.R. Hagen and T.W.B. Kibble, *Global conservation laws and massless particles*, Phys. Rev. Lett. **13** (1964) 585
- [9] P.W. Higgs, *Spontaneous symmetry breakdown without massless bosons*, Phys. Rev. **145** (1966) 1156
- [10] J. Goldstone, A. Salam and S. Weinberg, *Broken Symmetries*, Phys. Rev. **127** (1962) 965
- [11] The UA1 Collaboration, *Experimental observation of isolated large transverse energy electrons with associated missing energy at  $s = 540$  GeV*, Phys. Lett. B **122** (1983) 1
- [12] The UA2 Collaboration, *Observation of single isolated electrons of high transverse momentum in events with missing transverse energy at the CERN pp collider*, Phys. Lett. B **122** (1983) 5-6
- [13] The UA1 Collaboration, *Experimental observation of lepton pairs of invariant mass around  $95$  GeV/ $c^2$  at the CERN SPS collider*, Phys. Lett. B **126** (1983) 5
- [14] The UA2 Collaboration, *Evidence for  $Z^0 \rightarrow e^+e^-$  at the CERN pp collider*, Phys. Lett. B **129** (1983) 1-2
- [15] The ATLAS Collaboration, *Observation of a new particle in the search for the Standard Model Higgs boson with the ATLAS detector at the LHC*, Phys. Lett. B **716** (2012) 1 [arXiv:1207.7214v2]

- [16] The CMS Collaboration, *Observation of a new boson at a mass of 125 GeV with the CMS experiment at the LHC*, *Phys. Lett. B* **716** (2012) 1 [[arXiv:1207.7235v2](#)]
- [17] F.L. Wilson, *Fermi's Theory of Beta Decay*, *Am. J. Phys.* **36** (1968) 1150
- [18] B. Di Micco *et al.*, *Higgs boson potential at colliders: status and perspectives*, [arXiv:1910.00012v4](#) (2020)
- [19] The ATLAS Collaboration, *Constraints on the Higgs boson self-coupling from the combination of single-Higgs and double-Higgs production analyses performed with the ATLAS experiment*, *ATLAS-CONF-2019-049* (2019)
- [20] R. Abdul Khalek *et al.*, *Higgs Physics at the HL-LHC and HE-LHC*, *CERN Yellow Rep. Monogr.* **7** (2019) 221-584 [[arXiv:1902.00134v2](#)]
- [21] J. Strube, *Measurement of the Higgs Boson Coupling to the Top Quark and the Higgs Boson Self-coupling at the ILC*, *Nuclear and Particle Physics Proceedings* **273-275** (2016)
- [22] P. Roloff *et al.*, *Double Higgs boson production and Higgs self-coupling extraction at CLIC*, [arXiv:1901.05897v2](#) (2019)
- [23] B. Fuks, J.H. Kim and S.J. Lee, *Scrutinizing the Higgs quartic coupling at a future 100 TeV proton-proton collider with taus and b-jets*, *Phys. Lett. B* **771** (2017) 10 [[arXiv:1704.04298v2](#)]
- [24] A.S. Belyaev, P.B. Schaefer, and M.C. Thomas, *Precise test of Higgs properties via triple Higgs production in VBF at future colliders*, *Phys. Rev. D* **99** (2019) 015030 [[arXiv:1801.10157v1](#)]
- [25] S. Weinberg, *Phenomenological Lagrangians*, *Physica A* **96** (1979) 1-2
- [26] A.C. Longhitano, *Heavy Higgs bosons in the Weinberg-Salam model*, *Phys. Rev. D* **22** (1980) 1166
- [27] A.C. Longhitano, *Low-energy impact of a heavy Higgs boson sector*, *Nuc. Phys. B* **188** (1981) 1
- [28] T. Appelquist and C. Bernard, *Strongly interacting Higgs bosons*, *Phys. Rev. D* **22** (1980) 200
- [29] A. Dobado and M.J. Herrero, *Phenomenological lagrangian approach to the symmetry breaking sector of the standard model*, *Phys. Lett. B* **288** (1989) 4

- [30] A. Dobado and M.J. Herrero, *Testing the hypothesis of strongly interacting longitudinal weak bosons in electron-positron collisions at TeV energies*, *Phys. Lett. B* **233** (1989) 3-4
- [31] A. Belyaev *et. al.*, *Multi Higgs and Vector boson production beyond the Standard Model*, *JHEP* **2013** (2013) 5 [[arXiv:1212.3860v1](#)]
- [32] R. Contino *et. al.*, *Strong Double Higgs Production at the LHC*, *JHEP* **2010** (2010) 89 [[arXiv:1002.1011v2](#)]
- [33] The ATLAS Collaboration, *Combined measurements of Higgs boson production and decay using up to 80 fb<sup>-1</sup> of proton-proton collision data at  $\sqrt{s} = 13$  TeV collected with the ATLAS experiment*, *ATLAS-CONF-2019-005* (2019) [[arXiv:1909.02845v2](#)]
- [34] The ATLAS Collaboration, *Search for the  $HH \rightarrow b\bar{b}b\bar{b}$  process via vector-boson fusion production using proton-proton collisions at  $\sqrt{s} = 13$  TeV with the ATLAS detector*, *ATLAS-CONF-2019-030* (2019) [[arXiv:2001.05178v2](#)]
- [35] I. Brivio and M. Trott, *The Standard Model as an Effective Field Theory*, *Phys. Reports* **793** (2019) 27 [[arXiv:1706.08945v3](#)]
- [36] S. Di Vita *et. al.*, *A global view on the Higgs self-coupling*, *JHEP* **2017** (2017) 69 [[arXiv:1704.01953v2](#)]
- [37] R.L. Delgado *et al.*, *One-loop  $\gamma\gamma \rightarrow W_L^+W_L^-$  and  $\gamma\gamma \rightarrow Z_L Z_L$  from the Electroweak Chiral Lagrangian with a light Higgs-like scalar*, [arXiv:1404.2866v2](#) (2014)
- [38] G. Buchalla, O. Catà and C. Krause, *On the Power Counting in Effective Field Theories*, *Phys. Lett. B* **731** (2014) 4 [[arXiv:1312.5624v1](#)]
- [39] E. Arganda, C. García-García and M.J. Herrero, *Probing the Higgs self-coupling through double Higgs production in vector boson scattering at the LHC*, *Nuc. Phys. B* **945** (2019) 114687 [[arXiv:1807.09736v3](#)]
- [40] D. A. Dicus and H. He, *Scales of Fermion Mass Generation and Electroweak Symmetry Breaking*, *Phys. Rev. D* **71** (2005) 093009 [[arXiv:hep-ph/0409131v4](#)]
- [41] F. Maltoni, J.M. Niczyporuk and S. Willenbrock, *Scale of fermion mass generation*, *Phys. Rev. D* **65** (2002) 033004 [[arXiv:hep-ph/0106281v2](#)]
- [42] T. Hahn, *Generating Feynman diagrams and amplitudes with FeynArts 3*, *Comp. Phys. Comm.* **140** (2001) 3 [[arXiv:hep-ph/0012260v2](#)]
- [43] T. Hahn, M. Pérez-Victoria, *Automated one-loop calculations in four and D dimensions*, *Comp. Phys. Comm.* **118** (1999) 2-3 [[arXiv:hep-ph/9807565v1](#)]

- 
- [44] G. P. Lepage, *A new algorithm for adaptive multidimensional integration*, *Journal of Comp. Phys.* **27** (1978) 2
- [45] J. Alwall *et al.*, *The automated computation of tree-level and next-to-leading order differential cross sections, and their matching to parton shower simulations*, *JHEP* **2014** (2014) 79 [[arXiv:1405.0301v2](#)]
- [46] S. Dawson, *The effective W approximation*, *Nuc. Phys. B* **249** (1985) 1
- [47] D. Arominski *et al.*, *A detector for CLIC: main parameters and performance*, *CLICdp-Note-2018-005* (2018) [[arXiv:1812.07337v1](#)]
- [48] R. Contino *et al.*, *Strong Higgs Interactions at a Linear Collider*, *JHEP* **2014** (2014) 6 [[arXiv:1309.7038v2](#)]
- [49] R. Brun and F. Rademakers, *ROOT — An object oriented data analysis framework*, *Nuclear Instruments and Methods in Physics Research Section A: Accelerators, Spectrometers, Detectors and Associated Equipment* **389** (1997) 1-2